Master's Thesis

Academic Year 2021

Numerical investigation on electrical and thermal characteristics in organic semiconductor films from the aspect of variable range hopping

Graduate School of Science and Technology,
School of Integrated Design Engineering,
Keio University

Descouens Nicolas

81923362

A Master's Thesis
submitted to Graduate School of Science and Technology, Keio University
in partial fulfillment of the requirements for the degree of
MASTER of School of Integrated Design Engineering

Descouens Nicolas

Advisor: Professor Noda Kei

Abstract of Master's Thesis of Academic Year 2021

Numerical investigation on electrical and thermal characteristics in organic semiconductor films from the aspect of variable range hopping

Category: Science / Engineering

The localization of states in organic semiconductor have caused some troubles at providing a viable thermal and electric transport. Understanding better the process in organic semiconducor could help improve the performances of many devices. We propose in this thesis to study the Einstein relationship and thermal conduction in regard of doped semiconductors which could be usefull for both understanding carrier transport and heat transport and also to engineer more efficient devices.

From the standpoint of the Variable Range Hopping (VRH) theory, we will compute models for both electric conduction and diffusion for classic organic semiconductors to finally be able to assess the Einstein ratio. We will perform simulation to grasp the influence of some parameters: doping, field, carrier density, energetic disorder, Fermi level. The model predicts value in accordance with the precedent litterature for most que the quantities, excepted the temperature and the Fermi level. To confirm our electric model, we used pentacene hole-only data measured by a precedent student and have found the numerical values for reasonable field to be in range with what was measured.

The background developped for the electric conduction has also been used to predict thermal conduction values for both phonons and charge carriers. Our approximated model succeeded in obtaining reasonable values in range with the litterature.

A special attention has been dedicated into developping a performing model in Julia and improving the performances without harming the precision and accuracy of the model.

Acknowledgements

Table of Contents

List of Figures

Chapter 1

Introduction

1.1 Organic semiconductors

1.1.1 Background

For the past century, inorganic materials have been at the heart of the semiconductor industry, with element such as silicon, germanium or gallium arsenide. But the industry turned itself to new devices, and organics semiconductor are one of them. Their different set of properties: very flexible, low cost, less polluting helped them to gain more interest.

In 1977, the first highly conducting polymer was discovered: chemically doped polyacetylene [8]. Such material can be easily processed by techniques already know in the industry: vacuum evaporation, solution casting... But a better understanding and control of the self-assembly of molecules, as well as a booming research field, have greatly increased the performances, reaching the charge carrier mobility of amorphous silicon for some of them (fig. 1.1). The high diversity of geometry within the material allows a better tuning of the characteristic of the semiconductor to the use cases. One greater advance is the combination of both organic and inorganic molecules, particularly with perovskite. The high mobility of inorganic material combined with the more flexible geometry of organic ones make possible the creation of devices that reaches the performances of single-crystal silicon [19, 25].

This new development has been seen through the recent appearance of organic devices in the market. The more flagrant one is OLED devices, they offer a better usability (flexible screens) with increased performance (higher color fidelity,

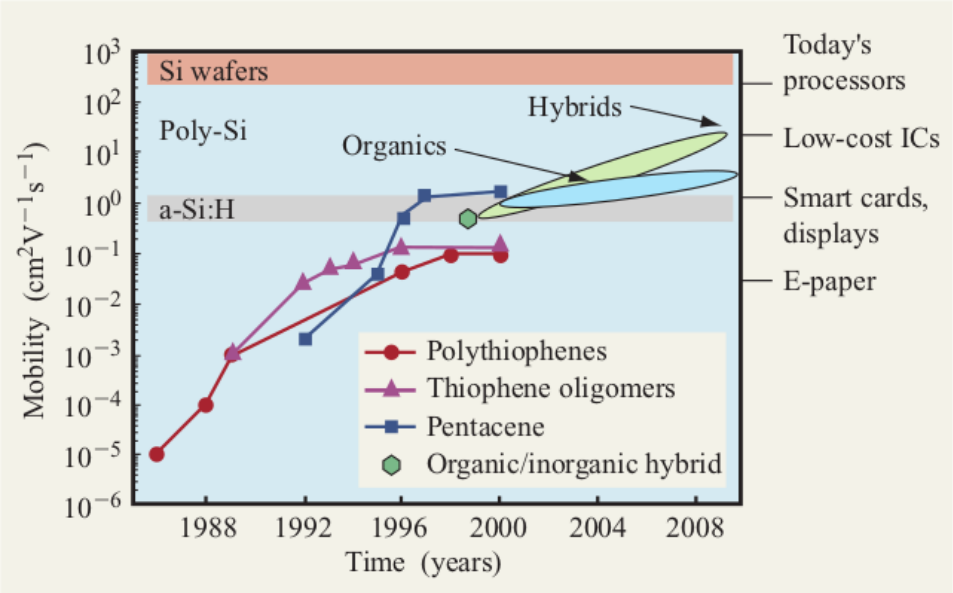

Figure 1.1: History of the evolution of mobility in organic semiconductors [25]

darker black and better contrast) better electric consumption. It's also used in professional devices such as OTFT [18], laser diode [23], ...

1.1.2 Future development

Organic semiconductor are overwhelmingly used in wearable and portable devices, mainly as screen using thin-films transistors. They offer an affordable, biodegradable, transparent, flexible alternative to the classic inorganic TFTs. However, one key characteristic for such device is the transit frequency, the highest frequency at which we can operate the transistor. Most organic material have a frequency of at most a few mega-hertz, which is not enough for modern devices which works at the gigahertz frequencies. Usually, higher operating frequency means a higher quality final product. Replacing inorganic TFTs by organic one could mean a lot for the industry as both p-channel and n-channel can be fabricated at room temperature. But the increase in performance as recently stalled and need further development and research to really reach the performances of the more classical inorganic semiconductors [33].

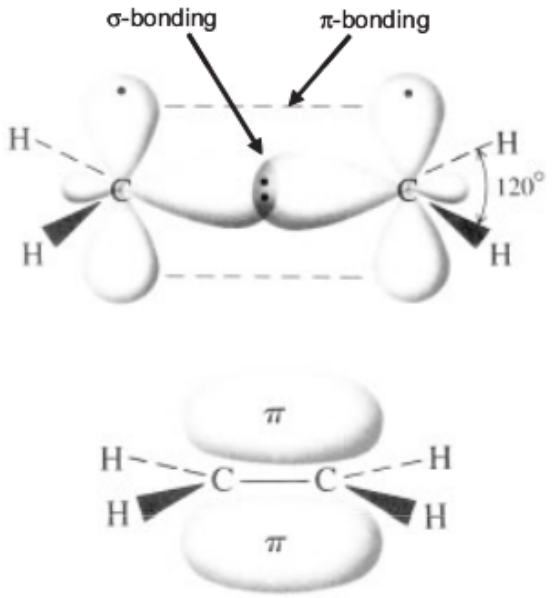

Figure 1.2: σ and π bonds in ethene [6]

1.1.3 Organic materials

Organic molecule are bound to each other by $\pi - \pi$ bounding which are the result of p_z-orbitals of sp^2-hybridized C-atoms in the molecules (fig. 1.2). Such bonding is way weaker compared to the classic σ-bounding in the molecule backbone. Therefore, the $\pi - \pi^*$ transitions have a typical lower gap: around $1.5\,\mathrm{eV} - 3\,\mathrm{eV}$ (fig. 1.3). Their crystallinity ranges from single-crystal (pentacene, rubrene crystals) [32] to completely amorphous semiconductors like α-NPD [28].

Those weaker Van der Waals bonding lead to more localized charge carrier in the material. Most of the time, charge carriers do not evolve in bands like in Si, but are subject to a HOMO (Highest Occupied Molecular Orbital) and LUMO (Lowest Unoccupied Molecular Orbital) states. It results in a much weaker wavefunction delocalization for the neighboring molecules [6]. Instead of band transport, organic materials are subject to hopping transport: a charge carrier hop from a site to an other and thus participate to the general conduction (fig.1.4). The difference between trapping and hopping state is in the recombination and release rate. if the former one is higher than the letter one, the state is a recombination center,

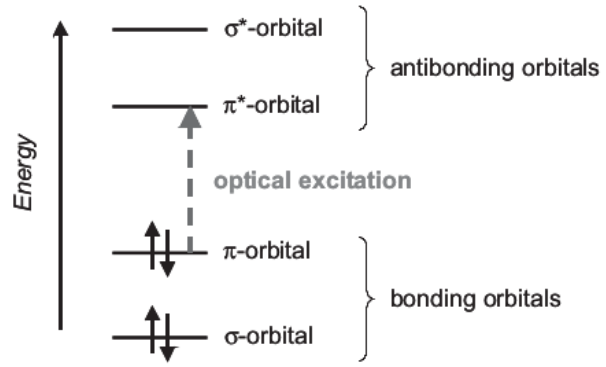

Figure 1.3: $\pi - \pi^*$ bonding [6]

otherwise, it is a trap. In this model the difference between trapping states and recombination states can be thin.

Organic semiconductors are divided between polymers and small molecules. The separation occurs at 1000 molecular weights. Small molecules can achieve high cristallinty but are less soluble in solvent, requiring dry processes such as vacuum deposit, which is more difficult and more costly. On the other hand, polymer are easier to made in organic solvents. Even though small molecules show better performances, they're less stable than polymer in atmospheric conditions.

1.1.4 Charge carrier transport

As it has been said before, disorganized organic semiconductors are the place of localized charge carrier transport, and in the 70's, a theory has been proposed involving tunneling between near states [1]. Such theory as been previously discovered by Mott based on the dependence of the mobility on the temperature: an increasing temperature leads to an increasing mobility. This relation has been verified in practical devices [1, 14].

In the variable range hopping theory (VRH), the displacement between two states for a charge carrier is determined only by the difference in energy W and in position R, thus highlighting the fact that our system is resolutely in 4D. On top of that, we assume that the system is so disordered that this two quantities are decoupled. The jump frequency is usually described by the Miller-Abrahams

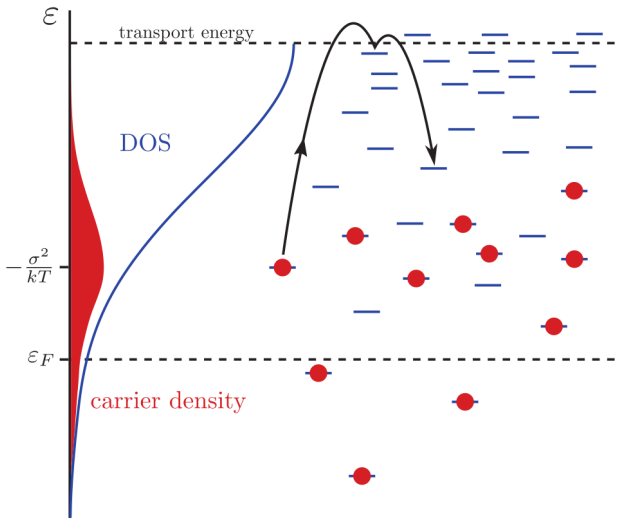

Figure 1.4: Hopping transport

formalism [17]:

$$\nu = \nu_0 \begin{cases} \exp\left(-2\alpha R_{ij} - \frac{E_j - E_i}{k_B T}\right) : E_j - E_i \geq 0 \\ \exp\left(-2\alpha R_{ij}\right) : E_j - E_i \leq 0 \end{cases} \tag{1.1}$$

- ν_0: base-jump frequency
- R_{ij}: distance between initial state i and final state j
- α: decay constant of the assumed hydrogen-like localized state wave functions
- E_i: energy of the state i

Depending on the position of the final state j, the formula changes. If the state is on higher energy, it requires tunneling to occur on the energetic part, whereas if the reaching state if of a lower energy, only the distance is taken into account for the tunneling effect, the jump being energetically favorable.

Using this formalism, it is possible to access the mobility and diffusivity for charge carrier.

1.1.5 The Einstein relation

It has been reported in organic semiconductor that the classical Einstein relation may be violated in certain conditions [13]. To better understand the changes in the Einstein ratio, we will first present the classic equation before explaining what can change.

Classical Einstein relation

$$\frac{D}{\mu} = \frac{k_b T}{q} \tag{1.2}$$

- μ: mobility
- D: diffusion
- k_B: Boltzmann constant
- T: temperature
- q: elementary charge

The Einstein relation [9], is a useful equation that link two quantities, μ and D over a simple equation. D constitutes a key parameter in analyzing semiconductor but is not so easy to measure. On the contrary, the mobility is easily accessed. However, in the presence of energetic disorder, such simple equation does not seem to hold [4, 21]. In non-equelibrium cases, it also seems that we can't use this relation anymore, the relation between the diffusion and the field seems to be quadratic [20].

Generalized equation

From the limit of the eq. 1.2, a new relation has been proposed, taking into account the dependence on the carrier concentration [22]:

$$\frac{D}{\mu} = \frac{n}{q\partial n/\partial E_F} \tag{1.3}$$

- E_F: quasi-Fermi level
- n: carrier concentration

With n being the carrier concentration defined by the fermi-dirac distribution $f = \frac{1}{1+exp\left(\frac{E-E_F}{k_B T}\right)}$ and g the gaussian density of state [22]:

$$n = \int_{-\infty}^{\infty} \frac{g(E)}{1 + \exp\left(\frac{E-E_F}{k_B T}\right)} dE \tag{1.4}$$

Such eq. 1.4 has been calculated following the hypothesis that drift and diffusion of charge carrier at fermi level are exactly compensated, meaning that there is no net current and is only valid for low electric field.

From this stating, a more suitable equation has been proposed in the following thesis.

1.1.6 Gaussian density of states

$$g(E) = \frac{N}{\sigma\sqrt{2\pi}} \exp\left(-\frac{E^2}{2\sigma^2}\right) \tag{1.5}$$

Gaussian density of states has been suggested by numerous monte-carlo simuations [7] as well by the observation of the excitonic absorption profile which is gaussian too. Besides, the intrinsic localization behavior of the gaussian density of state fit very well the observation made on real devices.

From a mathematical point of view, the disorder is directly linked to σ, which broadens the bell-shaped function (fig. 1.5, 1.6).

1.1.7 Thermal diffusion

Organic semiconductors have recently received much attention regarding their potential thermoelectric effect. From their figure of merit (eq. 1.6)

$$\mathrm{ZT} = \frac{\sigma \cdot S^2}{k} T \tag{1.6}$$

- S: Seebeck coefficient
- σ: electrical conductivity

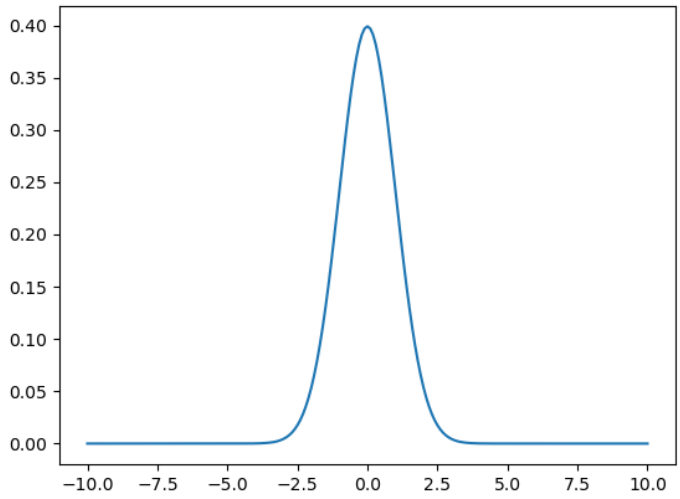

Figure 1.5: Gaussian DOS, $\sigma = 1$

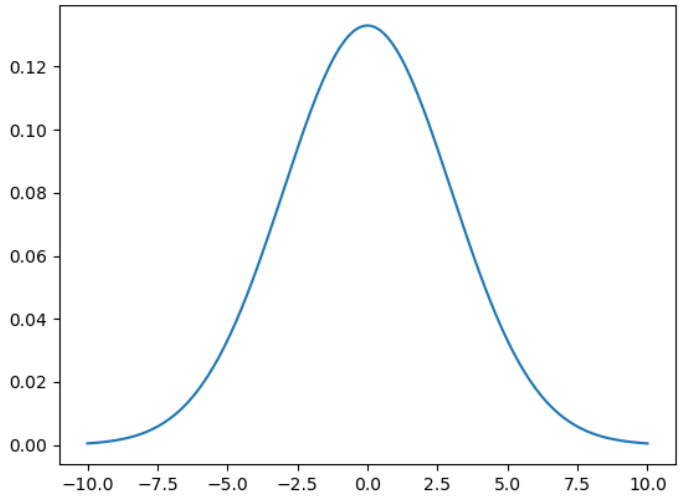

Figure 1.6: Gaussian DOS, $\sigma = 3$

- k: thermal conductivity

ZT value is representative of the device thermo-electric efficiency. A lower thermal conductivity k naturally leads to higher figure of merit and to an increased energetic conversion.

A better understanding of the thermo-electric behavior is key to engineering better devices, but the classical theory used on inorganic material [10] can't be applied directly to organic ones. The variety of morphology in organic semiconductors plays a great role in defining its thermal characteristics and is extremely sensitive to the spacial arrangement of the molecules within the material.

To simulate the thermal effect, one should take into account both charge carrier and phonon transport: $k = k_e + k_p$ with a slight predominance of the phonon in the process of thermal conduction [15].

1.2 Objectives of this thesis

The overall understanding of both electric and thermal behavior of organic semiconductors is scarce. Their great diversity, which is at the heart of their recent success, makes it difficult to get an accurate simulation of the charge carrier in the material. The goal of this thesis is to obtain, thanks to equations developed throughout the 20th century and to new hypothesis on the comportment of the charge carrier, as well as a powerful computer language, a reasonable approximation of the electric and thermal figures in doped organic semiconductors:

- Estimating Einstein ratio for many type of organic semiconductors
- Taking into account the doping behavior of the semiconductor, as well as the disorder and electric effect
- Estimating the thermal conduction by taking into account both charge carrier and phonon participation
- Simulating the model in a fairly small amount of time

The novelty of this study resides in the multitude of the parameters taken into account and in new behavior for charge carrier within the material.

Chapter 2

Electric properties

The framework for the electric properties: diffusion D, mobility μ and Einstein ratio η will be detailed in this section. As now on, we will adopt the following formalism. If not stated otherwise, every quantity written in lowercase will be reduced and all the quantity in uppercase will be the non-reduced equivalent (u_F is the reduced quantity of U_F). To reduce the unit we will use respectively for the energetic dimension and spatial dimensions:

$$\begin{aligned} u &= \frac{U}{k_b T} \\ r &= 2\alpha R \end{aligned} \tag{2.1}$$

k_B being the Boltzmann constant and $\alpha = 4.34 \times 10^7\,\mathrm{cm}^{-1}$ the decay constant of the assumed hydrogen-like localized state wave functions.

2.1 Gaussian formalism

To simulate the localized behavior of charge carrier, we will use a Gaussian density of states (Gaussian DOS) for doped semiconductor. The doping effect will take form of an another Gaussian with a different peak. The origin of the energy will be taken to be the LUMO level, but this theory works for holes and electron alike: an energy inversion is will bring us into the hole formalism.

$$g\left(E,\hbar\omega_\alpha\right) = \frac{1}{\sqrt{2\pi}}\left\{\frac{N_i}{\sigma_i}\exp\left(-\frac{\left(E-\hbar\omega_\alpha\right)^2}{2\sigma_i^2}\right) + \frac{N_d}{\sigma_d}\exp\left(-\frac{\left(E-\hbar\omega_\alpha+E_D\right)^2}{2\sigma_d^2}\right)\right\} \tag{2.2}$$

- $N_i(cm^{-3})$: density of charge carriers for the intrinsic material
- $N_d(cm^{-3})$: density of charge carriers for the doping material
- $\hbar\omega_\alpha(J)$: mode effect, vibration of the lattice
- $\sigma_i(J)$: width of the intrinsic Gaussian, representative of the disorder of the intrinsic material
- $\sigma_d(J)$: width of the doped Gaussian, representative of the disorder of the doped material
- $E_D(J)$: energy shift between intrinsic and doped material

g is expressed in $J^{-1}cm^{-3}$.

On the figure 2.1, the doping results in a broadening of the DOS, which is coherent with doping increasing the number of states within the material.

Using the Fermi-Dirac distribution, the carrier concentration is:

$$n = \int_{-\infty}^{+\infty} \frac{g_e(U)}{1+exp\left(\left(\frac{U-(\hbar\omega_\alpha+U_F)}{k_BT}\right)\right.}dU \tag{2.3}$$

2.2 Variable range hopping

2.2.1 Background

We suppose that the charge carrier jump by tunneling from one state to another. The system is thus described in 4 dimensions: 3 for the spatial dimension, and 1 for the energy.

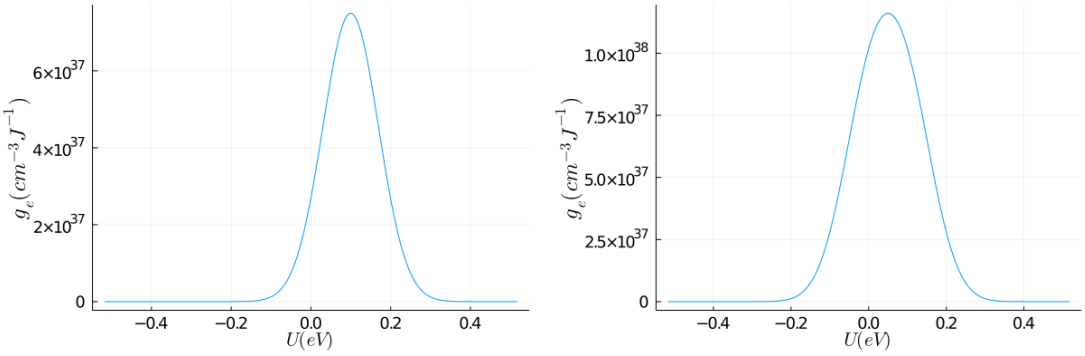

(a) Non-doped semiconductor

(b) Doped semiconductor
$N_d = 2.1 \times 10^{18}\,\mathrm{cm}^{-3}$, $E_D = 0.1\,\mathrm{eV}$

Figure 2.1: DOS doping comparison
$T = 300K$, $N_i = 2.1 \times 10^{18}\,\mathrm{cm}^{-3}$, $\hbar\omega_\alpha = 0.16 \times 10^{-19}\,\mathrm{J}$

In our semi-classical model, we define the average probability for a jump to be the geometrical mean for all the jump within a material:

$$\langle P \rangle = \lim_{n\to\infty} \left[\prod_i^n P_i\right]^{1/n} = \exp\left[\lim_{n\to\infty} \frac{1}{n}\sum_i^n \ln P_i\right] \tag{2.4}$$

P_i being a singular jump in the material, we make the average over all the jump in the material.

As the arithmetic mean is more familiar, it's easier to work with the $\frac{1}{n}\sum_i^n \ln P_i$ part. To do so, we define the distance hopped to be:

$$r_i = -ln(P_i) \tag{2.5}$$

The i arises from the fact that $P_i < 1$ and the logarithm is thus negative. Finally, we get:

$$\langle P \rangle = exp(-r_{nn}) \tag{2.6}$$

With r_{nn} being the average range to the nearest neighbor for each state throughout the material, it has the advantage of summarizing the spatial and energy distribution of the states in a single variable r_{nn}. The Miller-Abrahams hopping rate can now be written as:

$$\nu = \nu_0 \cdot exp(-r_{nn}) \tag{2.7}$$

Usually, ν_0, the basic hopping rate, is set to 1×10^{13} Hz.

If we define P_{ij} to be the probability of a jump from the state i to the state j, from an energetic standpoint:

$$P_{ij}^{energy} = exp\left(\frac{U_i - U_j}{k_B T}\right) = exp(u_i - u_j) \tag{2.8}$$

From a spatial standpoint:

$$P_{ij}^{spatial} = exp\left(-2\alpha L_{ij}\right) = exp(-l_{ij}) \tag{2.9}$$

We can fairly assume that:

$$P_{ij} = P_{ij}^{total} = P_{ij}^{energy} \cdot P_{ij}^{spatial} = e^{[u_i - u_j] - l_{ij}} = e^{r_{ij}} \tag{2.10}$$

We write the field effect as: $\beta = \frac{Fe}{2\alpha k_B T}$, F being the field intensity in $V cm^{-1}$. The course of a charge carrier is modified by the field. To model this, we include it directly in the equation of the 4D distance: a state alongside the field direction will be seen as closer or father depending on the angle θ between R_{ij} and F:

$$\left.\begin{array}{ll} R_{ij} & = (1 + \beta\cos\theta)L_{ij} + (U_j - U_i) \quad \text{for } U_j > U_i - \beta\cos\theta R_{ij} \\ & = L_{ij} \qquad\qquad\qquad\qquad\quad \text{for } U_j < U_i - \beta\cos\theta R_{ij} \end{array}\right\} \tag{2.11}$$

$(1 + \beta\cos\theta)$ arises from the shift of the fermi level due to the field (fig. 2.2). We assume here that for states to lower energy, only the physical distance is taken into account as the charge carrier does not need to make a jump to higher energies.

2.2.2 Nearest neighbor

The quantity r_{nn} can be computed thanks to the formula of the "number of free states" $\mathscr{N}$: the mean number of free state at a distance $\mathscr{R}$ [1] of a certain point in the material. We suppose that the material is disorganized enough to make both energetic and spatial dimension uncorrelated, and that the states are equally distributed in respect of the Gaussian DOS.

$$\mathcal{N}(u,T,\beta,\mathscr{R}) = \int_0^{\pi}\int_0^{\mathscr{R}}\int_{-\infty}^{\mathscr{R}+u-r(1+\beta\cos\theta)} g(v)\left[1-F(v)\right]\frac{k_BT}{8\alpha^3} \times 2\pi r^2\sin\theta dv dr d\theta \tag{2.12}$$

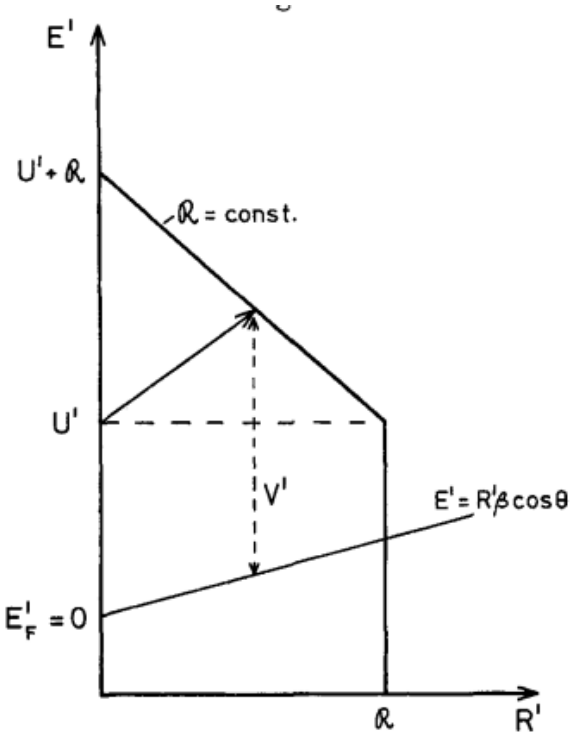

Figure 2.2: Energetic-spatial relationship (source [1])

$g(1-F)$ represents the emptiness of a state, F being the Fermi-Dirac equation, $1-F$ is the probability of the state to be empty, i.e a state where a charge carrier can jump. $\frac{k_BT}{8\alpha^3}$ is simply a reducing factor to get rid of the $g(1-F)$ unit. $4\pi r^2$ is the surface of a sphere with a radius r and $\frac{1}{2}\sin\theta$ makes the average between the

field effect direction and the direction of r. The $\frac{1}{2}$ factor arises from the integral $\int_0^\pi \frac{1}{2}\sin\theta = 1$. The born in the energetic integral $\mathscr{R}+u-r(1+\beta\cos\theta)$ corresponds to the maximum energetic value for a jump of distance $\mathscr{R}$. Finally, $\mathcal{N}$ computes the number of states enclosed in a 4D sphere of radius $\mathscr{R}$.

We thus define r_{nn} as the radius at which we found, in average, 1 free state i.e $\mathcal{N}(r_{nn}) = 1$.

This method for computing $\mathscr{N}$ is similar to the percolation criteria $\mathcal{N}(r_{nn}) = B_c$ with $B_c = 2.8$ being the percolation criteria. When the percolation theory intends to find a series of jump within the material, our r_{nn} quantity means the nearest free states, which intuitively corresponds to the distance at which we find 1 state.

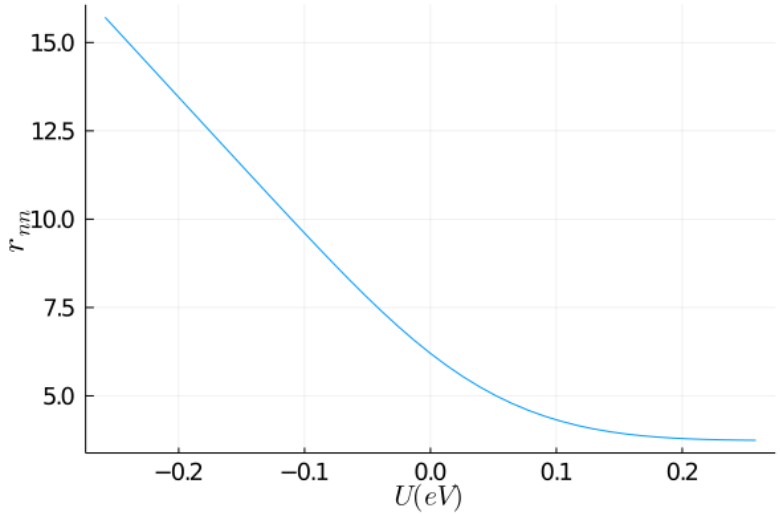

Figure 2.3: r_{nn} behavior for pentacene, $F = 5.3\,\mathrm{V\,cm^{-1}}$ (pentacene parameters appendix A)

From the figure 2.3, we see that for low value of energy, the quantity r_{nn} skyrockets. The rarefaction of free states due to both the reduction of the density thanks to the Gaussian DOS and the filling the Fermi-Dirac distribution mean that for a charge carrier to find an available spot is harder. On the opposite, we see a plateau at higher energetic values. The filling of the states is very low and at such energy, charge carrier can make energetically favorable jump to lower states. Mathematically, the born $\mathscr{R} + u - r(1 + \beta\cos\theta)$ makes it happen: for lower u, $\mathscr{R}$ compensate to cover the spectrum $g(1 - F)$, and for higher energy, u alone is

enough to cover it.

2.2.3 Real hopped distance

With r_{nn}, we have an insight of the geometry of the material, but what really matters to find the diffusion or mobility is the average displacement of the charge carrier, that we will name x_F. Of course, such quantity is affected by the field intensity.

We first define:

$$\begin{aligned}
I_1 &= \int_0^{\pi} \int_{u-r_{nn}\beta\cos\theta}^{u+r_{nn}} g(v)\left[1-F(v)\right]\left[\frac{r_{nn}-v+U'}{1+\beta\cos\theta}\right]^3 \sin\theta\cos\theta dv d\theta \\
I_2 &= \int_0^{\pi} \int_{-\infty}^{u-r_{nn}\beta\cos\theta} g(v)\left[1-F(v)\right] r_{nn}^3 \sin\theta\cos\theta dv d\theta \\
I_3 &= \int_0^{\pi} \int_{u-r_{nn}\beta\cos\theta}^{u+r_{nn}} g(v)\left[1-F(v)\right]\left[\frac{r_{nn}-v+U'}{1+\beta\cos\theta}\right]^2 \sin\theta dv d\theta \\
I_4 &= \int_0^{\pi} \int_{-\infty}^{u-r_{nn}\beta\cos\theta} g(v)\left[1-F(v)\right] {r_{nn}}^2 \sin\theta dv d\theta
\end{aligned} \tag{2.13}$$

And the distance written as:

$$x_F = \frac{I_1 + I_2}{I_3 + I_4} \tag{2.14}$$

The eq. 2.14 is a weighted mean. I_1 and I_3 represent jumps to state of higher energy, thus involving not only the distance but the energy. I_2 and I_4 represent jumps to state of lower energy, thus involving only the spatial distance hopped.

$\left[\frac{r_{nn}-v+U'}{1+\beta\cos\theta}\right]$ is comparable to a distance. If we take the expression $v = r_{nn} + u - r(1+\beta\cos\theta)$ from the eq. 2.12, we find for the distance r:

$$r = \left[\frac{r_{nn}-v+U'}{1+\beta\cos\theta}\right] \tag{2.15}$$

Moreover, to understand better the role of this integral, it is better to split it in two parts. First:

$$w = g(v)\left[1 - F(v)\right]\left[\frac{r_{nn} - v + U'}{1 + \beta\cos\theta}\right]^2 \sin\theta dv \tag{2.16}$$

This represents the number of free state at a certain distance r.

The function $f(v) = \left[\frac{r_{nn}-v+U'}{1+\beta\cos\theta}\right]\cos\theta$ represents the distance to a free state pondered by the field effect $\cos\theta$.

Finally, we can sum up the relation 2.14 by:

$$x_F = \frac{\int_{V_1} f(v)w(v) + \int_{V_2} f(v)w(v)}{\int_{V_1} w(v) + \int_{V_2} w(v)} \tag{2.17}$$

With V_1 and V_2 being the surface of integration.

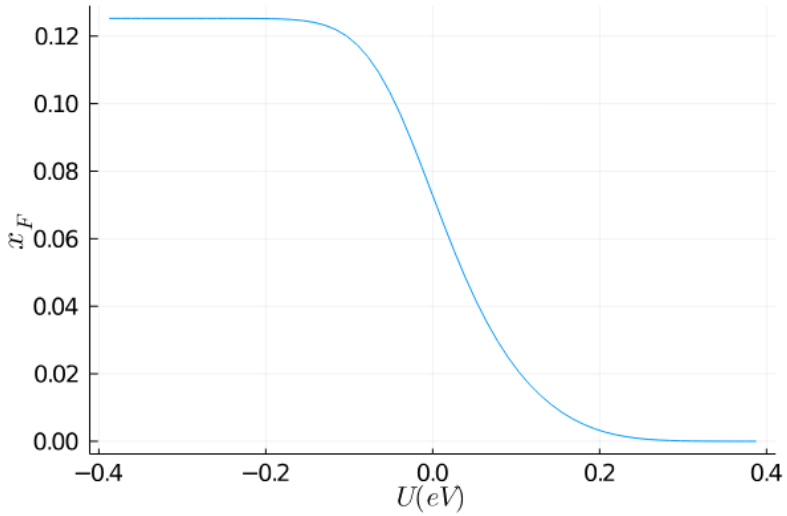

Figure 2.4: x_F dependence on energy, $F = 5.3\,\mathrm{V\,cm^{-1}}$ (pentacene parameters appendix A)

The energy dependency (fig. 2.4) see two plateaus, one a high energy is 0, meaning that at this level, most of the jump are made only downward in energy. For the

negative energies, the depletion in free state due to the Fermi-Dirac distribution and the Gaussian DOS make the jump longer. But it reaches a plateau because at a certain point, the jump is made in energy to reach more state dense energetic levels.

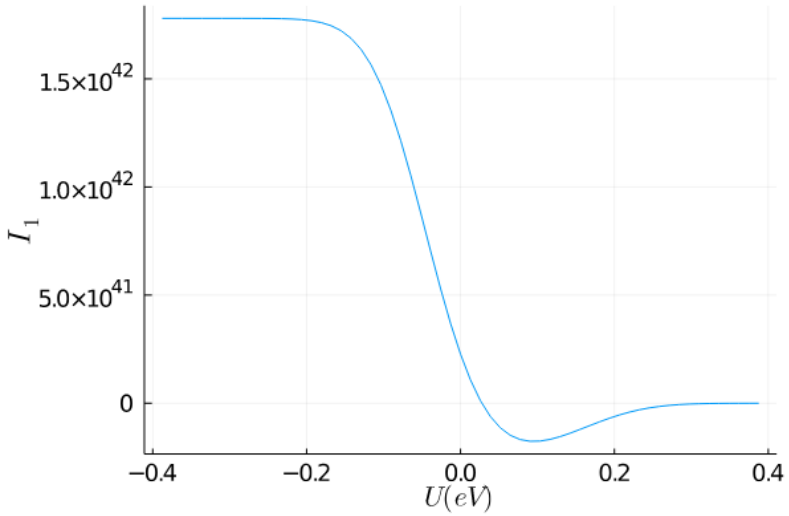

Figure 2.5: I_1 dependence on energy, $F = 5.3\,\mathrm{V\,cm^{-1}}$ (pentacene parameters appendix A)

By looking a little bit more into detail on I_1 and I_2 (fig. 2.5, 2.5), we can justify mathematically the global behavior of x_F. I_2 is similar to a Gaussian bell because $g(1-F)$ dominates the integral. However, for I_1, for positive values we have indeed the lower born of the integral that $u - r_{nn}\beta\cos\theta$ that goes beyond the high density zone of states. Concerning the lower values, the increase of r_{nn} compensate the decrease of energy u, making the upper limit $u + rnn$ more or less constant.

By studying the influence of the field on x_F (fig. 2.7), we see that its response is linear regarding low fields. We notice that $\lim_{x\to 0} xf = 0$. Indeed, if the charge carrier is not influenced by an electric field, its surrounding is isotropic, thus the jump are equidistant regarding all the direction and there is no preferable direction jumped.

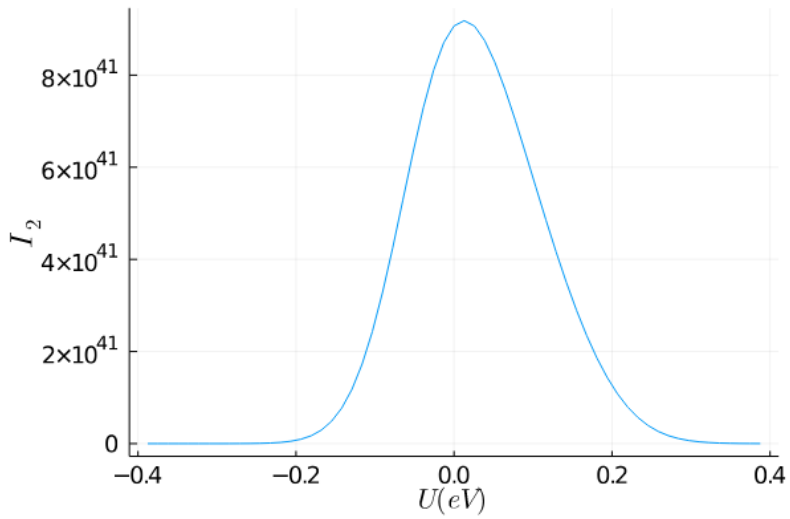

Figure 2.6: I_2 dependence on energy, $F = 5.3\,\mathrm{V\,cm^{-1}}$ (pentacene parameters appendix A)

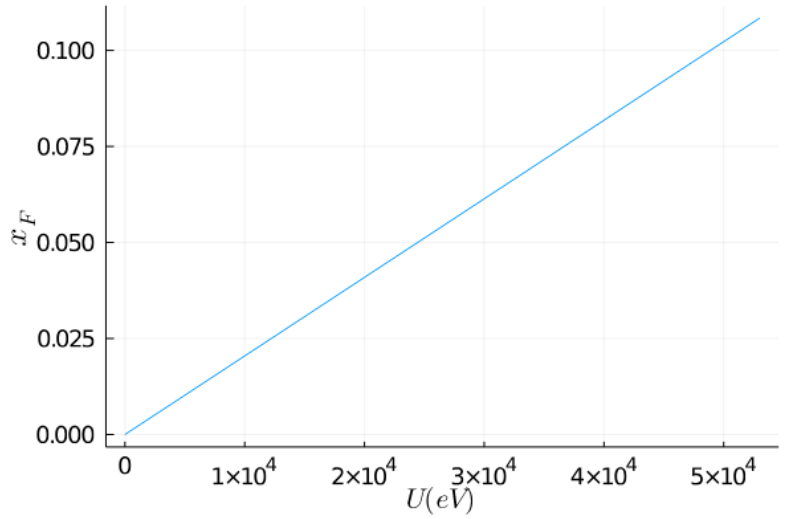

Figure 2.7: x_f dependence on the field, $F = 5.3 \times 10^4\,\mathrm{Vcm^{-1}}$ (pentacene parameters appendix A)

2.2.4 Mobility

Mobility is classically defined as the average velocity of the particle divided by the force. In our case, the mean distance jumped being x_F and a particle jumps

at a rate $\nu_0 e^{-r_{nn}}$(eq. 2.7):

$$\mu = \frac{\langle x \rangle}{F} = \frac{\nu_0 X_F e^{-r_{nn}}}{F} \tag{2.18}$$

From the equation 2.18, we can plot the mobility depending on the energy (figure 2.8). At low energy, the charge carrier find it difficult to move because there is a decrease in available states and so they can't participate to the mobility. However, at higher energy, we already noticed that the jump are made in great majority regarding the energy and not regarding spatial coordinates. Thus the mobility for higher value drops to 0 too. The global shape is very similar to a Gaussian bell.

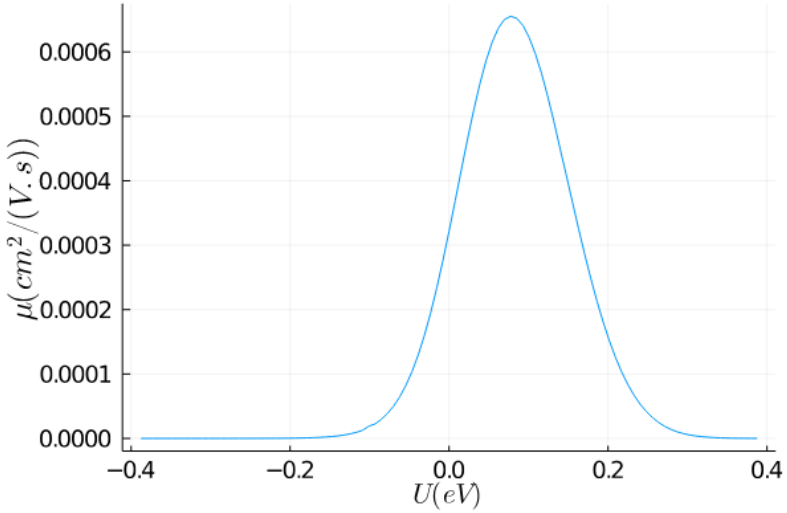

Figure 2.8: μ dependence on the energy, $F = 5.3\,\mathrm{V\,cm^{-1}}$ (pentacene parameters appendix A)

From the formula 2.18, we can compute the conductivity σ:

$$\sigma(U) = q g_e(U) F(U) \mu(U) k_B T \tag{2.19}$$

We see on the figure 2.9 that the curve is shifted toward LUMO level. The majority of the available states being situated near this level, it is natural for the conductivity to do the same.

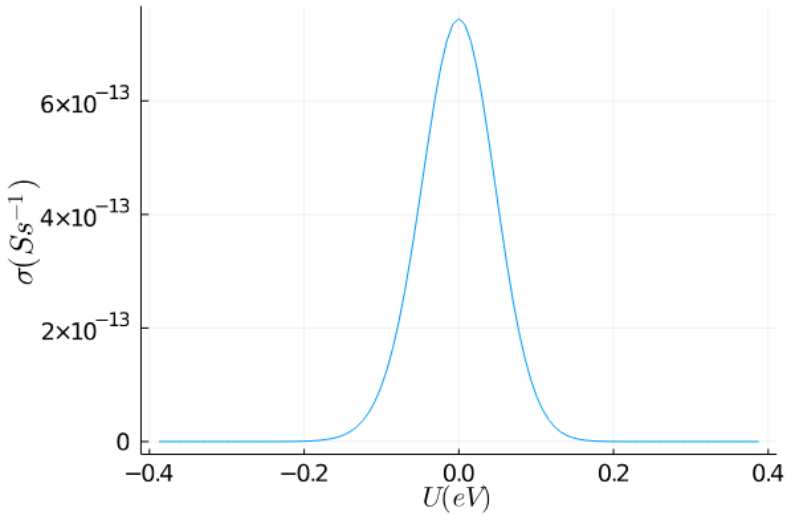

Figure 2.9: σ dependence on the energy, $F = 5.3\,\mathrm{V\,cm^{-1}}$ (pentacene parameters appendix A)

Of course the mobility is only defined for a sample affected by a field.

We define the global mobility in the material as $\mu(u)$ weighted by the number of states:

$$\mu = \frac{\int_{-\infty}^{+\infty} \mu(u)g(u)F(u)du}{\int_{-\infty}^{+\infty} g(u)F(u)du} \tag{2.20}$$

In a similar way, we define:

$$\sigma = \frac{\int_{-\infty}^{+\infty} \sigma(u)g(u)F(u)du}{\int_{-\infty}^{+\infty} g(u)F(u)du} \tag{2.21}$$

2.2.5 Stochastic variance of time

Stochastic variance of time, i.e the variance of the trapping time, is an essential concept for the diffusion. For higher t, we will greater trapping effect in the material. However, even though $t = 0\,\mathrm{s}$, it doesn't mean that the material is exempt of trap. t being an average, their effect becomes negligible. The equation

is similar to x_f (eq. 2.14):

$$t = \frac{T_1 + T_2}{T_3 + T_4} \tag{2.22}$$

We define T_1, T_2, T_3, T_4 as follow:

$$\begin{aligned}
T_1(u) &= \int_0^{\pi} d\theta \sin\theta \int_0^{r_{nn}} dr 2\pi r^2 \int_{u-r\beta\cos\theta}^{r_{nn}+u-r(1+\beta\cos\theta)} d\epsilon \\
&\quad \times \frac{g(u)(1-F(v))}{v_0} \exp\left((1+\beta\cos\theta)r + \epsilon - u\right), \\
T_2(u) &= \int_0^{\pi} d\theta \sin\theta \int_0^{r_{nn}} dr 2\pi r^2 \int_{-\infty}^{u-r\beta\cos\theta} d\epsilon \frac{g(u)(1-F(v))}{v_0} \\
&\quad \times \exp((1+\beta\cos\theta)r) \\
T_3(u) &= \int_0^{\pi} d\theta \sin\theta \int_0^{r_{nn}} dr 2\pi r^2 \int_{u-r\beta\cos\theta}^{r_{nn}+u-r(1+\beta\cos\theta)} d\epsilon g(u)(1-F(v)), \\
T_4(u) &= \int_0^{\pi} d\theta \sin\theta \int_0^{r_{nn}} dr 2\pi r^2 \int_{-\infty}^{u-r\beta\cos\theta} d\epsilon g(u)(1-F(v))
\end{aligned} \tag{2.23}$$

Similarly to eq.2.13, $g(1-F)$ represents the emptiness of the arrival state. the exponential part can be summarized as: $exp(-r-u)$ and $\nu_0^{-1}exp(-r-u)$ represents the period of a jump. The range and the principle of the fraction is the same as for eq. 2.13. Here again, I_2 differs from I_1 at it doesn't take into account the energy part: the jump is downward in energy and is favorable.

From the fig. 2.10, we see that the time of a jump reaches low value for high energy. From what has been previously deduced, at high energy the jumps (which are rare), occurs solely on the energy level. For lower value, states being farther away, it is harder to escape a trap.

2.2.6 Diffusivity

From the definition of the diffusion, we have:

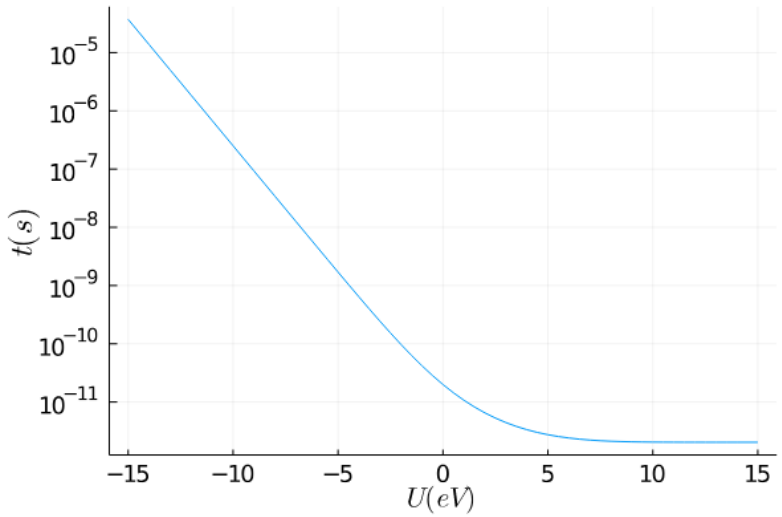

Figure 2.10: t dependence on the energy, $F = 5.3 \times 10^4\,\mathrm{V\,cm^{-1}}$ (pentacene parameters appendix A)

$$D = \frac{1}{2 \cdot n} \frac{d}{dt} \langle x^2(t) \rangle \tag{2.24}$$

- $\langle x(t) \rangle$: average displacement of a particle
- $n = 3$: dimension of the system, in our case

However, in presence of an electric field, a drift term appears in the equation 2.24:

$$D = \frac{1}{2 \cdot n} \frac{d}{dt} \langle (X(t) - \langle X(t) \rangle)^2 \rangle \tag{2.25}$$

$(X(t) - \langle X(t) \rangle$ is the drift of a certain displacement regarding the mean value. In a similar manner to eq. 2.18, we get:

$$
\begin{aligned}
D &= \frac{1}{2 \cdot n} \left\langle (X(t) - \langle X(t) \rangle)^2 \right\rangle \nu_0 e^{-r_{nn}} \\
D &= \frac{1}{6} \left\langle X(t)^2 - 2X(t)\langle X(t) \rangle - \langle X(t) \rangle^2 \right\rangle \nu_0 e^{-r_{nn}} \\
D &= \frac{1}{6} \left(\langle X(t)^2 \rangle - 2\langle X(t) \rangle \langle X(t) \rangle - \langle X(t) \rangle^2 \right) \nu_0 e^{-r_{nn}} \\
D &= \frac{1}{6} \left(\langle X(t)^2 \rangle - \langle X(t) \rangle^2 \right) \nu_0 e^{-r_{nn}}
\end{aligned}
\tag{2.26}
$$

We define ΔX as the average displacement around the average position $\langle X \rangle$ in a way that: $X = \langle X \rangle + \Delta X$. ΔX is the pure randomness rising from the charge displacement. If we substitute X^2 by this new relation in eq. 2.26, we obtain:

$$
\begin{aligned}
D &= \frac{1}{6} \left([\langle X \rangle + \Delta X]^2 - \langle X \rangle^2 \right) \nu_0 e^{-r_{nn}} \\
D &= \frac{1}{6} \left(\langle X \rangle^2 + 2\langle X \rangle \Delta X + (\Delta X)^2 - \langle X \rangle^2 \right) \nu_0 e^{-r_{nn}} \\
D &= \frac{1}{6} \left(2\langle X \rangle \Delta X + (\Delta X)^2 \right) \nu_0 e^{-r_{nn}}
\end{aligned}
\tag{2.27}
$$

ΔX is the movement non-influenced by the field and $\langle X \rangle = X_F$.

The quantity $t\nu_0 e^{-r_{nn}}$ models the number of jumps made by a charge carrier. We can tie this frequency to the stochastic time of trap:

$$
\frac{1}{\nu} = \frac{1}{\bar{\nu}} \pm t \tag{2.28}
$$

We introduce the average hopping rate: $\bar{\nu} = \nu_0 e^{-r_{nn}}$. Thanks to a power series, we can approximate the hopping frequency to:

$$
\nu = \bar{\nu} \pm \bar{\nu}^2 t \tag{2.29}
$$

As a charge carrier is subject to displacement assisted with field X_F, it is also subject to a random diffusive movement best represented with the R_{nn} which we assume is less influenced by the field:

$$\begin{aligned} X_d &= \nu R_{nn} \\ &= \bar{\nu}(R_{nn} \pm \Delta R) \\ \Delta R &= \bar{\nu} t R_{nn} \end{aligned} \tag{2.30}$$

We assume that the average displacement around the average $\Delta X = R_{nn} \pm \Delta R$. By using the new expressions we obtained into equation 2.26:

$$\begin{aligned} D &= \frac{1}{6}\left(2\langle X\rangle(R_{nn} \pm \Delta R) + (R_{nn} \pm \Delta R)^2\right)\nu_0 e^{-r_{nn}} \\ &\textbf{The average of } 2\langle X\rangle(R_{nn} \pm \Delta R) = 2X_F \Delta R \\ D &= \frac{1}{6}\left(2X_F\Delta R + (R_{nn} \pm \Delta R)^2\right)\nu_0 e^{-r_{nn}} \\ D &= \frac{1}{6}\left(2X_F\Delta R + R_{nn}^2 \pm 2R_{nn}\Delta R + (\Delta R)^2\right)\nu_0 e^{-r_{nn}} \\ D &= \frac{1}{6}\left(2X_F\Delta R + R_{nn}^2 \pm 2R_{nn}\Delta R + (\Delta R)^2\right)\nu_0 e^{-r_{nn}} \\ D &= \frac{1}{6}\left(2X_F\Delta R + R_{nn}^2(1 \pm 2\bar{\nu}t) + (\Delta R)^2\right)\nu_0 e^{-r_{nn}} \end{aligned} \tag{2.31}$$

We make multiple assumptions. First $2\bar{\nu}t \ll 1$ and the variations of $(\Delta R)^2$ are very small compared to R_{nn}^2. These two assumptions are based on the small variation around R_{nn}. Finally:

$$D = \frac{1}{6}(2X_F t\nu_0 e^{-r_{nn}} + R_{nn}^2)\nu_0 e^{-r_{nn}} \tag{2.32}$$

From the figure 2.11, we see that for higher energy levels, D is higher. It is consistent with the precedent theory as with higher energy, particles have way more possibility to move. In 2.32, we introduced ΔX which is the average deviation from the displacement and gives the constant value for higher energy as r_{nn} also takes into account the energy part of the jumps.

In the same fashion as with the mobility, the diffusivity is defined throughout the material by:

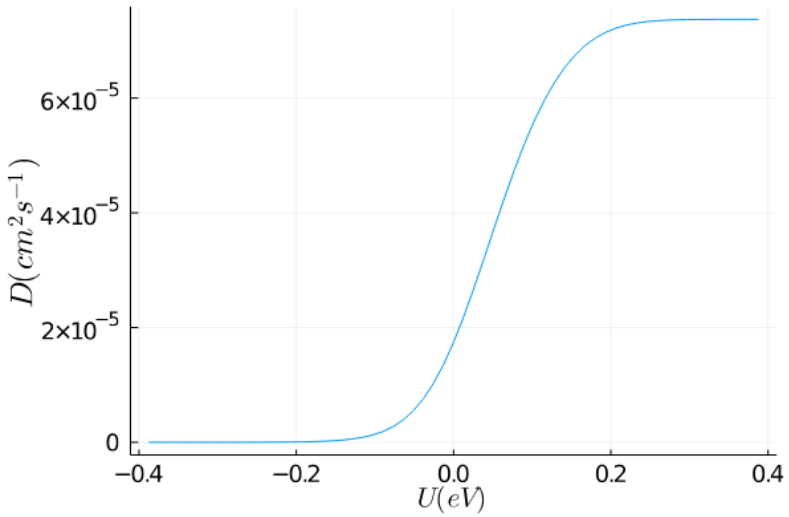

Figure 2.11: D dependence on the energy, $F = 5.3\,\mathrm{V\,cm^{-1}}$ (pentacene parameters appendix A)

$$D = \frac{\int_{-\infty}^{+\infty} D(u)g(u)F(u)du}{\int_{-\infty}^{+\infty} g(u)F(u)du} \tag{2.33}$$

2.2.7 Einstein ratio

From the precedent values we computed, we can now define the Einstein ratio as we will use it. Fist, the energy dependent one writes as:

$$EinsteinRatio(u) = \frac{D(u)}{\mu(u)} \tag{2.34}$$

However, as the relation is usually referred to its original equation (eq. 1.2), we will define η as:

$$\eta(u) = \frac{D(u)}{\mu(u)}\frac{q}{k_B T} \tag{2.35}$$

From the figure 2.12, we see that the Einstein ratio attains a minimum for energy around the LUMO level. The value quickly rises for lower and higher energy

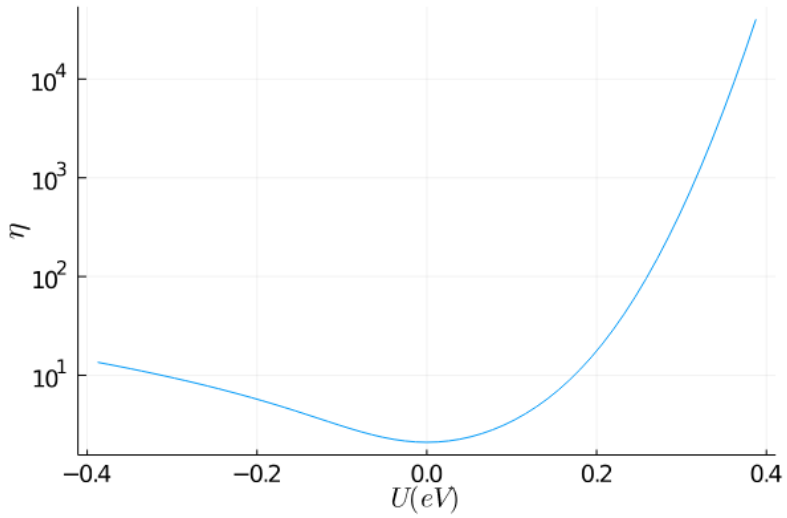

Figure 2.12: η dependence on the energy, $F = 5.3\,\mathrm{V\,cm^{-1}}$ (pentacene parameters appendix A)

level. For lower energy, it is admitted that traps cause higher η value. For greater energies, the quick decrease of the mobility due to the lack of spatial displacement as well as the constant D value due to the average variation of displacement ΔX, helps η ratio value to rise quickly.

2.2.8 Summary of some numerical value

To assess the viability of our model, we will perform some computation on the global values of μ, D, and η.

We performed a computation with $F = 4 \times 10^4\,\mathrm{Vcm^{-1}}$, to respect the value measured in Xavier's thesis [12].

	$\mu(\mathrm{cm \cdot V^{-1} \cdot s^{-1}})$	$D(\mathrm{cm \cdot s^{-1}})$	η
Values measured	2.15×10^{-5}	2.85×10^{-6}	5.1
Simulation	8.9×10^{-5}	5.45×10^{-6}	3.38

The order of magnitude for the simulated values are comparable. However, the final simulated value η is a bit low compared to the real one measured. The overall mobility simulated is too high compared to the real one. It's due to a

under-evaluated deep traps presence in the Gaussian DOS. We also considered only energetic traps and spatial trap could be considered to reduce the overall mobility.

Chapter 3

Extensive simulation

3.1 Parameters influence on Einstein

Now that we have introduced all the parameters and equation for the electric part in our model, we can start to study the effect of different parameters on it.

3.1.1 Electric Field

Field is a predominant parameters in various devices, from diodes to transistor. It is also easy to measure as a difference of voltage.

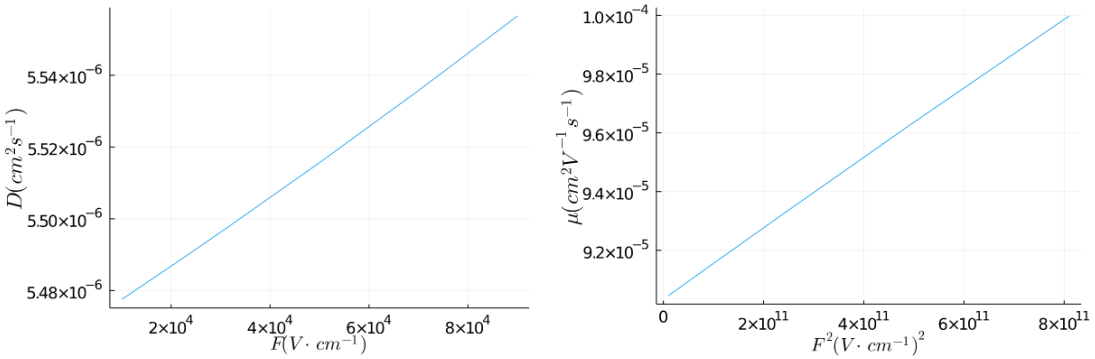

(a) D dependence on low field (pentacene parameters appendix A)

(b) μ dependence on low field (pentacene parameters appendix A)

For lower field ($\sim 1 \times 10^4\,\mathrm{V \cdot cm^{-1}}$), we observe a linearity for D (fig. 3.1a). Regarding the mobility, we clearly see a quadratic dependence on the field (fig. 3.1b). However, if we look closer at the numerical value, we can notice that for lower field the mobility is more or less constant. At the end, thanks to a constant

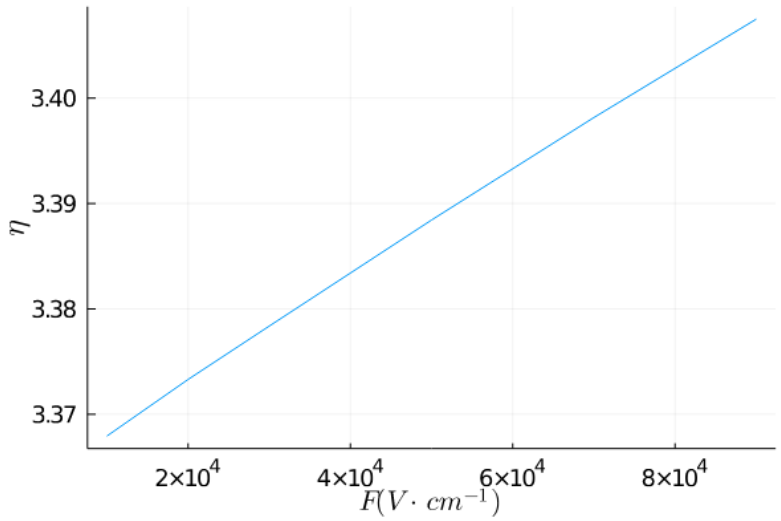

Figure 3.2: η dependence on low field (pentacene parameters appendix A)

mobility and a linear diffusivity regarding the field, the η value follow the tendency of D and is linear regarding low fields..

By increasing the field ($\sim 1 \times 10^5\,\mathrm{V \cdot cm^{-1}}$), we can observe a new behavior for the electric characteristics (fig. 3.3a, 3.3b, 3.4).

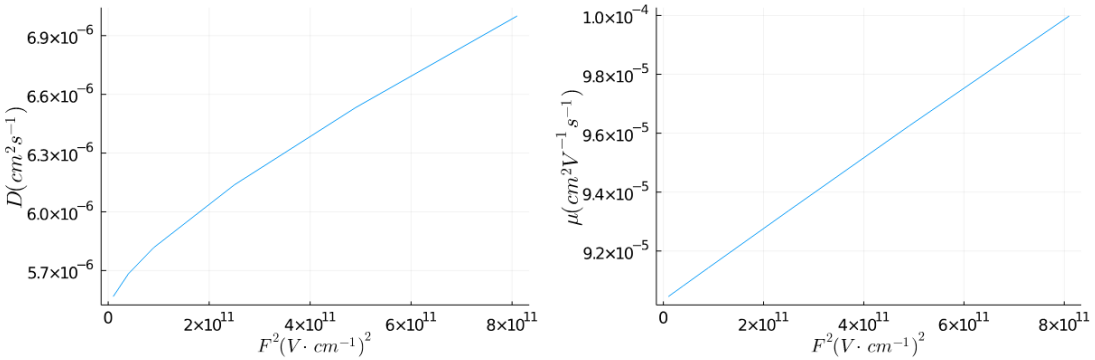

(a) D dependence on high field (pentacene parameters appendix A)

(b) μ dependence on high field (pentacene parameters appendix A)

Indeed, the diffusivity D starts having quadratic behavior, as described in the paper [13]. While the mobility still has a quadratic behavior (fig. 3.3b), it seems that the increase is greater for the μ value and that the Einstein ratio η sees a

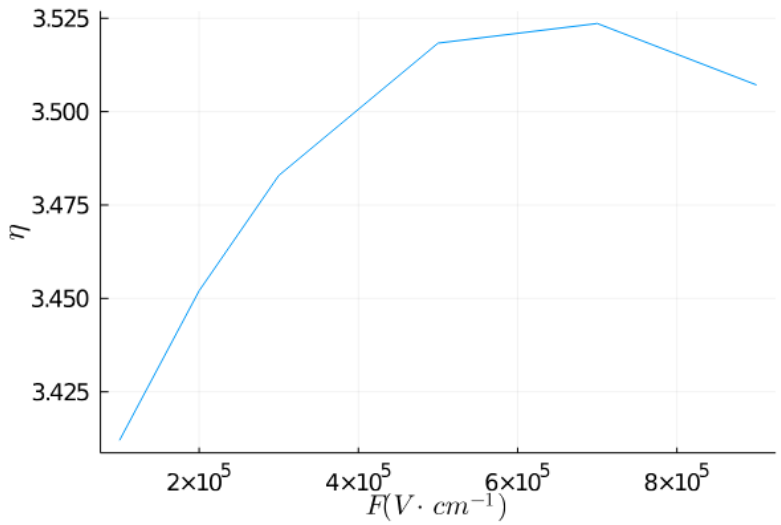

Figure 3.4: η dependence on high field (pentacene parameters appendix A)

local maximum for higher field (fig. 3.4).

3.1.2 Temperature

The classic Einstein relation makes it dependent on the energy with a $\frac{1}{T}$ ratio. However, on our simulation, we saw that the η relation was increasing with lower temperature (fig. 3.6). If we look closely to the dependence of μ and D (fig. 3.5a and 3.5b) over the temperature, we remark that it decreases with lower temperature, which seem logical. However, at the end it seems that the diffusivity reduces more slowly compared to the mobility. Such dependence can also be found in the paper [13]. One explanation would be the increase in the influence of deep traps. The strong localized states at low temperatures impaired the drift movement due to the mobility.

By looking more thoroughly at the conductivity for higher T value (fig. 3.5b), we remark that the curve follows roughly a linear dependence regarding $T^{-1/4}$ value. This relation has been proved to be the Mott dependence [2]. We see that the relation is not exactly linear, but from the simplification we made for the computation (reduced range, see chapter 4), we can suppose that the relation is sufficiently verified.

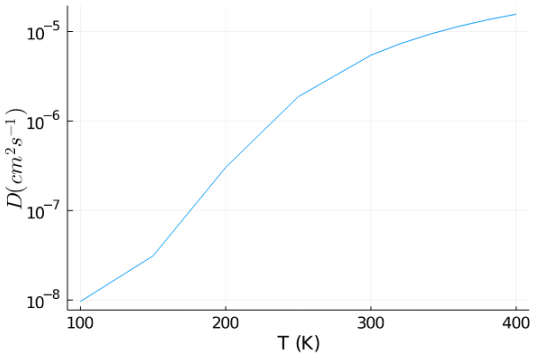

(a) D dependence on T (pentacene parameters appendix A)

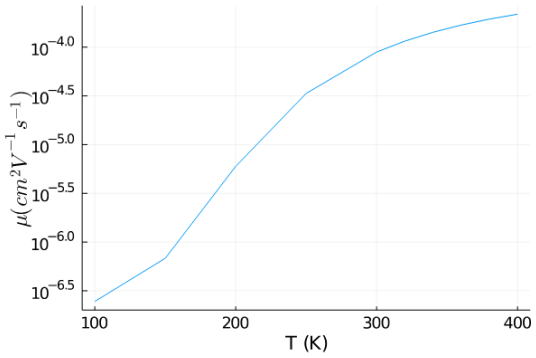

(b) μ dependence on T (pentacene parameters appendix A)

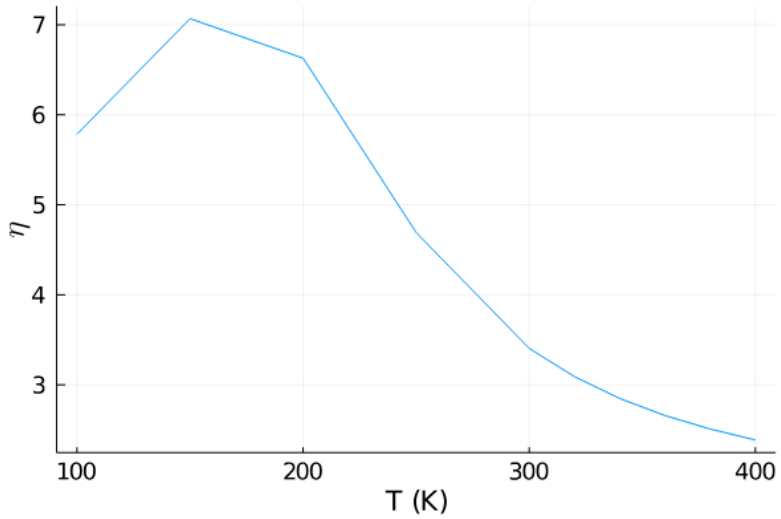

Figure 3.6: η dependence on T (pentacene parameters appendix A)

3.1.3 Charge carrier concentration

There are multiple ways of assessing the influence of the carrier concentration:

- Changing N_i: it can be performed in a field effect transistor by changing the gate voltage [30].
- Changing the Fermi level. By increasing it further to LUMO level, one can facilitates the passage of electrons to the LUMO level, thus changing

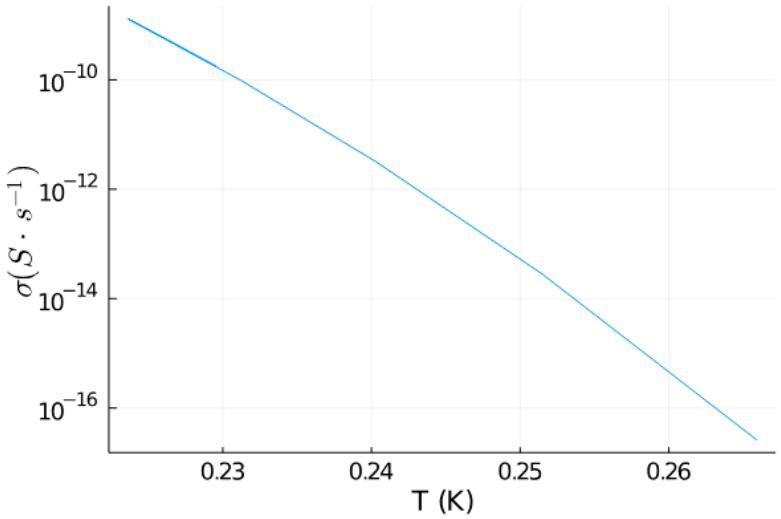

Figure 3.7: σ dependence on T (pentacene parameters appendix A)

the number of charge carrier. Such thing can be done by doping, by the impurities.

- Changing the energetic disorder of the semiconductor. Like the Fermi level, such change on the DOS is performed by introducing new molecules in the semiconductor. These molecules being wanted or simply impurities.

We will assess the influence of such parameters in a purely theoretic point of view, as it is very difficult to measure such quantities isolated from the other one. It is indeed very difficult to increase the N_i quantity without changing the energetic disorder or the Fermi level, as it as been observed in [30].

Fermi level influence

The simulation was performed with the following parameters:

- $\sigma_i = 0.1\,\mathrm{eV}$
- $N_i = 3 \times 10^{21}\,\mathrm{cm}^{-3}$
- $F = 5.3 \times 10^{4}\,\mathrm{Vcm}^{-1}$
- $T = 300\,\mathrm{K}$

An increase in Fermi level allows the charge carrier to escape the deep tail traps and to rise to higher energy levels. At such level the drift mobility becomes predominant compared to the diffusion current.

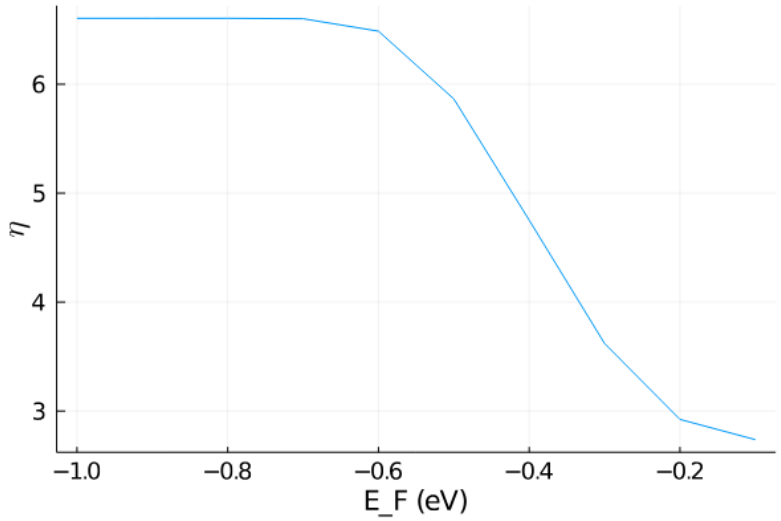

Figure 3.8: η dependence on E_F

On figure 3.8, we see that the Fermi level reaches a limit at which a getting closer to LUMO level means increasing the mobility in place of the diffusivity. Indeed, on the figure 3.9 that the decrease in Einstein ratio corresponds roughly to an exponential increase in charge carrier. Meaning that they reached higher energy level with more free states available.

Energetic disorder

We performed the simulation with the following parameters:

- $N_i = 3 \times 10^{21}\,\mathrm{cm}^{-3}$
- $E_F = -0.5\,\mathrm{eV}$
- $F = 5.3 \times 10^{4}\,\mathrm{Vcm}^{-1}$
- $T = 300\,\mathrm{K}$

We remark that increasing the energetic disorder increases immediately the Ein-

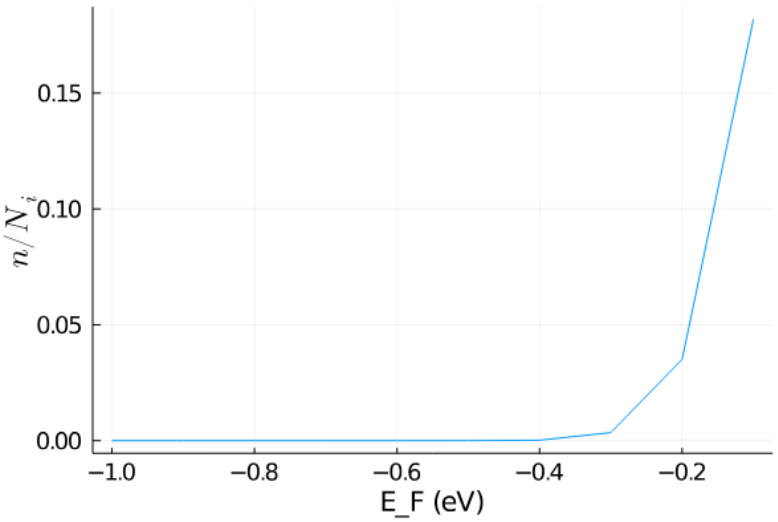

Figure 3.9: Number of charge carrier normalized on N_i

stein ratio (fig. 3.10). By spreading the state, we facilitate the diffusion process. Indeed, such movement is very sensitive to changes in DOS geometry: as the diffusion mainly occurs in all the direction, the change in volume of the DOS is very significant.

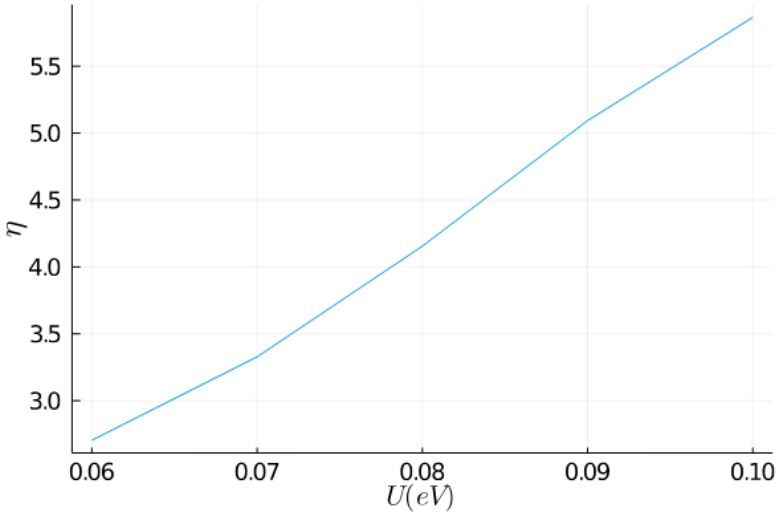

Figure 3.10: Dependence of η on energetic disorder σ

Carrier density

The DOS is also greatly affected by a change in carrier density N_i. Such changes should bring more states available in all the energy spectrum. We measured the influence of the change of carrier density by computed the charge carrier number:

$$n = \int_{-\infty}^{+\infty} g(U)F(U)dU \tag{3.1}$$

If all the other parameters stay the same, an increase in N_i results in a global increase in g, and thus to a global increase in charge carrier.

On figure 3.11, we see that the Einstein ratio increases with more carrier carrier n and with more N_i. The diffusion is way more sensitive to change in Gaussian topology and mobility is more sensitive to input of new charge carriers. Here, it seems that the input of charge carrier is predominant compared to the change in DOS structure.

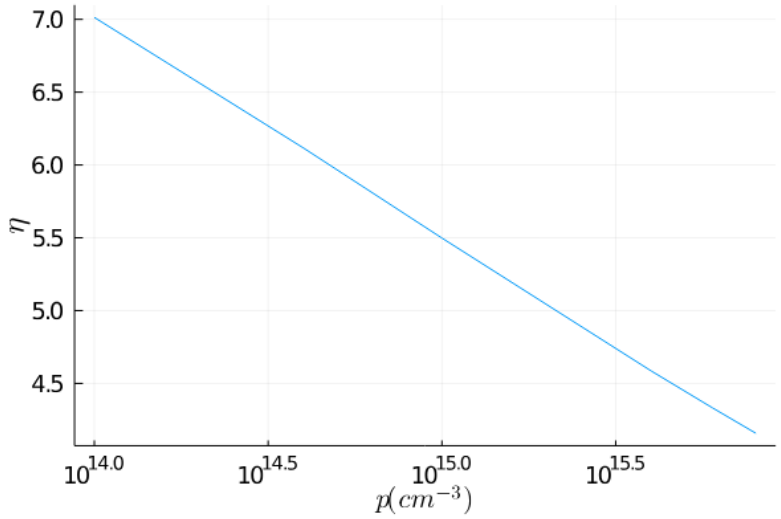

Figure 3.11: Dependence of η on carrier density N_i

3.2 Doping effect on Einstein relation

Because we used from the beginning a model of doped Gaussian DOS, we're now able de easily perform computation on doped semiconductor. We'll use α-NPD material doped with F4TCNQ (appendix B). To fully understand the behavior of doped material, we will perform the simulation over a whole range of quantity.

3.2.1 Effect of doping on the semiconductor

As explained before, the DOS is heavily changed by the dopant, it gives both new free states and brings new charge carrier to the material, changing the response of diverse parameters.

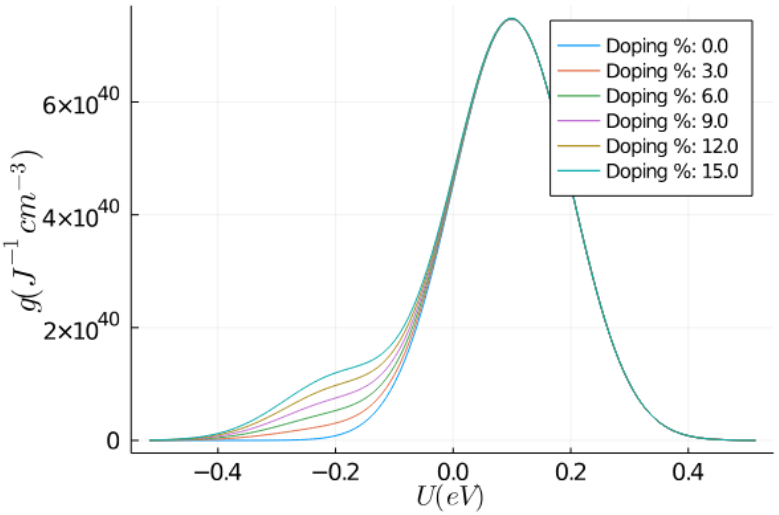

Figure 3.12: *DOS* dependence on the dopant quantity

As shown on fig. 3.19, an increase in dopant means the appearance of a second Gaussian peak in lower energy and in what is the forbidden gap. Of course more dopant means a higher peak. It is noted that doping a semiconductor heavily affects its DOS, and that the range of integration should appropriately be changed (chapter 4).

Such an heavy change on the DOS means that r_{nn}, the quantity describing the geometry of the semiconductor, will also be affected. The new states available

translates to the range to the nearest neighbor by reducing its value in the whole energy spectrum (fig. 3.13). Because the Fermi level is deep enough, there should be more significant states brought by the dopant than charge carrier.

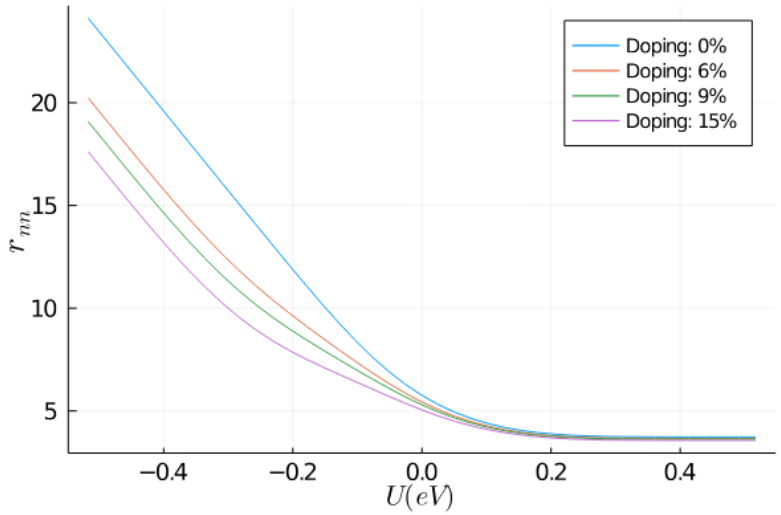

Figure 3.13: r_{nn} dependence on the dopant quantity

From the r_{nn} quantity, we compute x_F (fig. 3.14). When r_{nn} describes the semiconductor both in distance and energy, x_F only represents it from the spatial point of view. Here again, the behavior is greatly changed: in lower energy, the states are filled whereas in mid-range energy, x_F is reduced because there are more states available.

Doping also greatly affects the trapping effect. If we take solely into account the trapping time, we see that for increasing dopant concentration, we have lower values (fig. 3.15). It seems that doping decreases trapping influence at lower energy.

With lower stochastic trapping time, one could imagine that the assisted diffusion will be positively affected by the doping.

Indeed, if we look on the diffusivity curve (fig. 3.16a), we see a global increase for all the energy levels available. The same conclusion applies for the mobility μ (fig. 3.16b) but restricted around LUMO level, which corresponds roughly to the

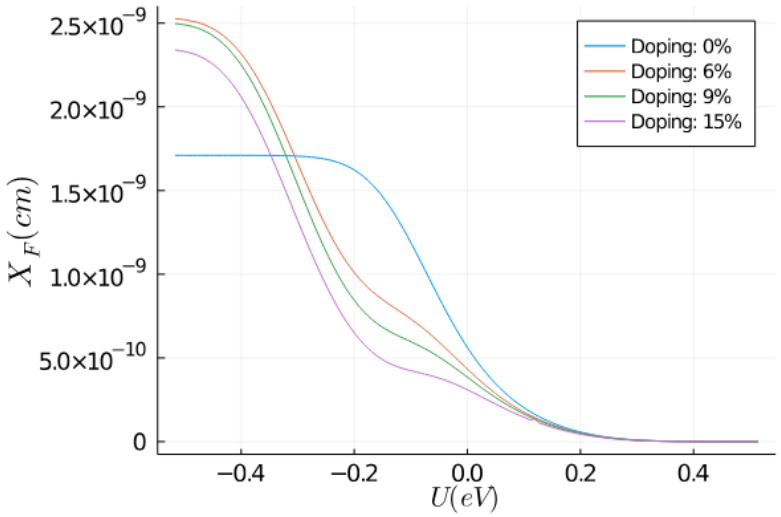

Figure 3.14: x_F dependence on the dopant quantity

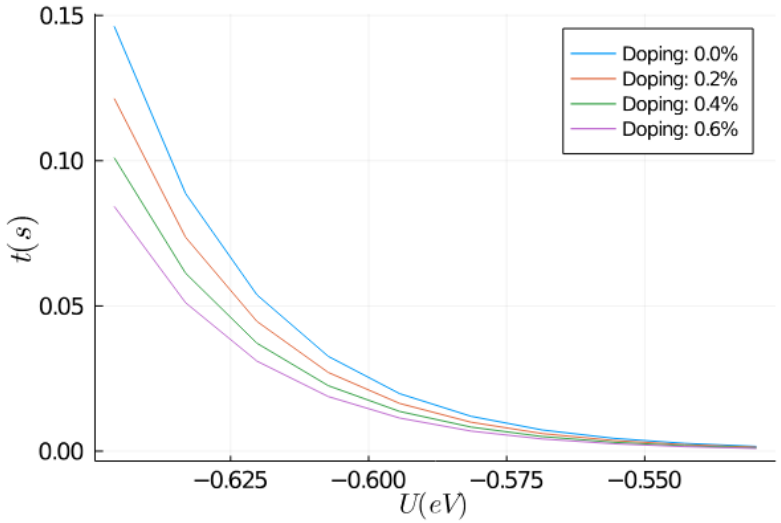

Figure 3.15: t dependence on the dopant quantity

energy of the new states added through the doping.

Finally, the Einstein ratio varies greatly between the pristine and the doped α-NPD (fig 3.17): it increases quite a lot. It can be explained by the deep changes that the DOS has experienced. The increase in new states really benefits the dif-

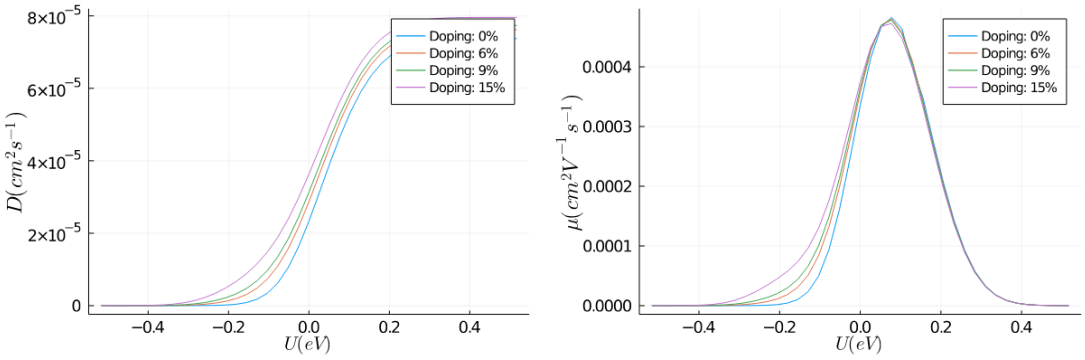

(a) D dependence on the dopant quantity (b) μ dependence on the dopant quantity

fusion as the charge carrier have more possibilities to scatter. However, between materials with comparable DOS morphology (the material with increasing doping), the major change comes from the increase in charge carrier density. This increases benefits the mobility as we see that the Einstein ratio decreases with higher dopant.

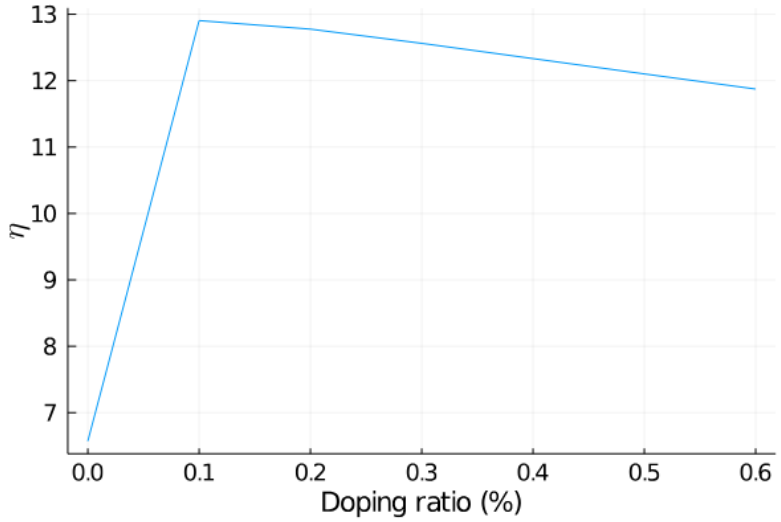

Figure 3.17: η dependence on the dopant quantity

3.2.2 Real device

On a precedent student work, hole-only pentacene diode fabricated with PEDOT:PSS and silver as electrode using vacuum evaporation process in order to

assess their Einstein ratio [12]. It was assumed that the ideality factor matched the Einstein ratio in such diode. Following what the precedent student measured in his work, we could extract the following values for the pentacene:

- $T = 300K$
- $E_F = 0.7\,\mathrm{eV}$
- $\sigma = 0.07$
- $N_i = 3 \times 10^{21}\,\mathrm{cm}^{-3}$

With the precedent parameters and the precedent data, we could plot the figure 3.18

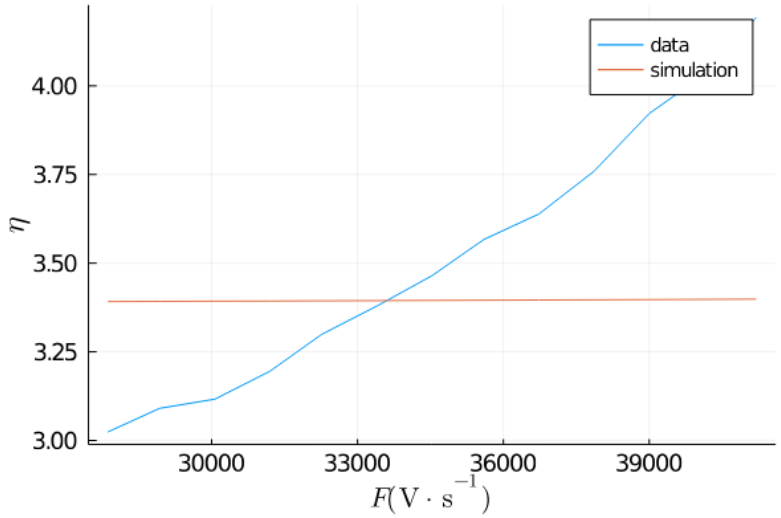

Figure 3.18: Simulated η compared to real value with varying field

The simulated values obtained are of a similar order of magnitude compared to the on obtained on real devices. However, the variation following the field F seems to be too slow. One possible explanation could be the lack of trapping effect on the mobility.

3.3 Thermal conduction

Thermal conduction is bore by both charge carriers and phonons however their behavior differs a lot. In the following part we will study both phonon and charge carrier transport regarding thermal characteristics.

3.3.1 Phonon transport

From the literature, it has been seen that for low frequencies phonon, a truncated Gaussian DOS fits real devices behavior [24]. To simulate the truncated DOS, we will reduce the frequency of integration during the computation of k_p

$$g_p\left(E, \hbar\omega_\alpha\right) = \frac{1}{\sqrt{2\pi}} \frac{N_{i-e}}{\sigma_i} \exp\left(-\frac{\left(E - \hbar\omega_\alpha\right)^2}{2\sigma_i^2}\right) \tag{3.2}$$

The parameters of the DOS 3.2 are the same as for the pristine electric Gaussian DOS. The material possesses the same features in term of phonon and charge carrier. Indeed, it has been observed [26] that the phonon displacement can be summed up by a series of jump between non propagating states. Besides, the usual vibration of a material is modeled by a discrete part [3] and a continuous part. We will here make the assumption that it can be simplified to a Gaussian DOS.

Diffusivity

Acoustic phonons, the one that participate to the energy propagation, are deemed to be at low frequency and to quickly reach a plateau (fig. 3.19).

However, this behavior is a rough approximation and usually the phonon diffusion sees some discrete characteristics. But, in order to simplify and get an approximate result, we will assume such constant diffusion. To obtain an estimate of the value, we will base ourselves on the average diffusion for amorphous SiO_2:

$$D_p = 4.10 \times 10^{-6}\,\mathrm{m^2 s^{-1}} \tag{3.3}$$

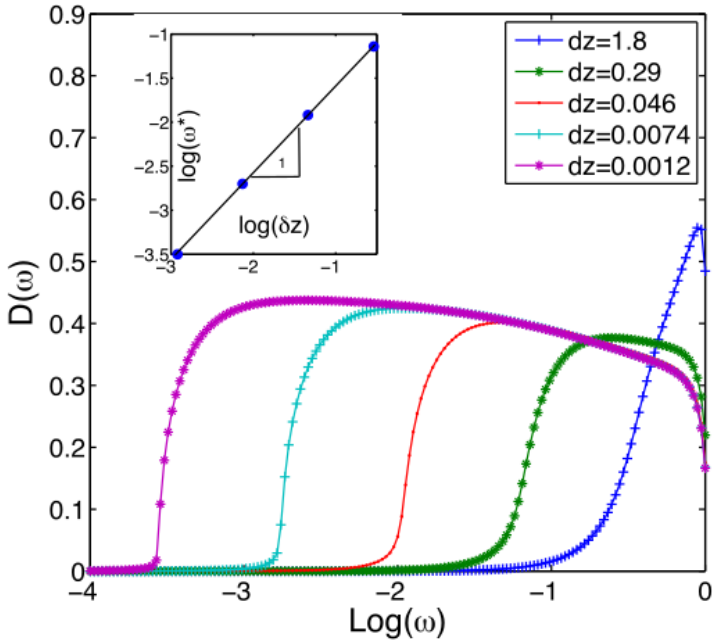

Figure 3.19: D dependence on the frequency ([31])

Conduction

Usually, the thermal conduction is defined as [27]:

$$k_p = \frac{1}{V} \sum_i C_i(T) D_i \tag{3.4}$$

- i: summation over all the vibrational modes
- V: volume of the system
- Ci: spectral heat capacity
- D_i: thermal diffusivity

However, to simplify eq. 3.4, we will make the average over the frequencies [16]:

$$k_p = \int_{\omega_{min}}^{\omega_{max}} g'(\hbar\omega)C(\hbar\omega)D(\hbar\omega)d\omega \tag{3.5}$$

Please note that in equation 3.5, the DOS g' is given "in frequency": the unit is $\mathrm{Hz}^{-1}\mathrm{cm}^{-3}$. The spectral heat capacity is defined by:

$$\begin{aligned} C(\hbar\omega) &= \hbar\omega \frac{\partial d}{\partial T}\left[\left(e^{\frac{\hbar\omega}{k_B T}} - 1\right)^{-1}\right] \\ C(\hbar\omega) &= \hbar\omega \frac{e^{\frac{\hbar\omega}{k_B T}}}{\left(e^{\frac{\hbar\omega}{k_B T}} - 1\right)^2} \end{aligned} \tag{3.6}$$

In eq. 3.5, we defined a range for the integral through ω_{min} and ω_{max}. We first defined the spatial frequencies to be $400\,\mathrm{cm}^{-1}$ and $4000\,\mathrm{cm}^{-1}$ leading to frequencies of 1.2×10^{13} Hz and 1.2×10^{14} Hz.

To make it work better with our model, we translated the frequency equation to the reduced energy one. First:

$$g'(\hbar\omega) = \hbar g(\hbar\omega) \tag{3.7}$$

By applying the change of variable $u = \frac{\hbar\omega}{k_B T}$:

$$k_p = k_B T \times \int_{u_{min}}^{u_{max}} g(u)C(u)D(u)du \tag{3.8}$$

3.3.2 Charge carrier transport

It has been demonstrated that charge carrier also participates to the heat conduction in semiconductors [5]. Such process arises because electron-hole pairs tend to be created at the hod end of the material and drift to the cold end, thus transmitting their energy.

It has been decided to use the same eq. 3.4 but with the charge carrier quantities D and g_e (eq. 2.32, 2.2). However, whereas for the phonons, only a small part

of the frequencies were involved in the conduction process, for the electron we assume that all the frequencies participates to it. It also translate in the energy spectrum, thus:

$$k_e = k_B T \left(\int_{-\infty}^{0} g_e(u) C(u) D_e(u) du + times \int_{0}^{+\infty} g_e(u) C(u) D_e(u) du \right) \quad (3.9)$$

Of course, as explained in section 4.4.2, to enhance the performances, we used a reduced range to frame the energy levels where the charge carrier are.

3.3.3 Parameters influence

Like what has been done in chapter 2 with the Einstein ratio, we will perform the same sort of study on the thermal conduction.

Temperature

Of course the thermal conduction is influenced by the temperature. According to eq. 3.8 and 3.9, there should be at least a linear increase in thermal conduction, which is verified in the simulations (fig. 3.20). The larger phonon conduction is verified in the literature [15]. The order of magnitude for the phonon conduction seems to be also verified in the literature, but the charge carrier one seems too low. Besides, in the paper [15], it seems that the thermal conduction does not exactly follows a linear dependence regarding the temperature like in our simulations.

Field

Only conduction by charge carrier is affected by the field. From the literature [15], the thermal conduction is constant for low fields and start to diverges at very high field value. We simulated that the charge carrier thermal conduction decreases with higher fields (fig. 3.21).

However, it should be noted that the equation for computing the thermal conduction for charge carriers takes into account a highly

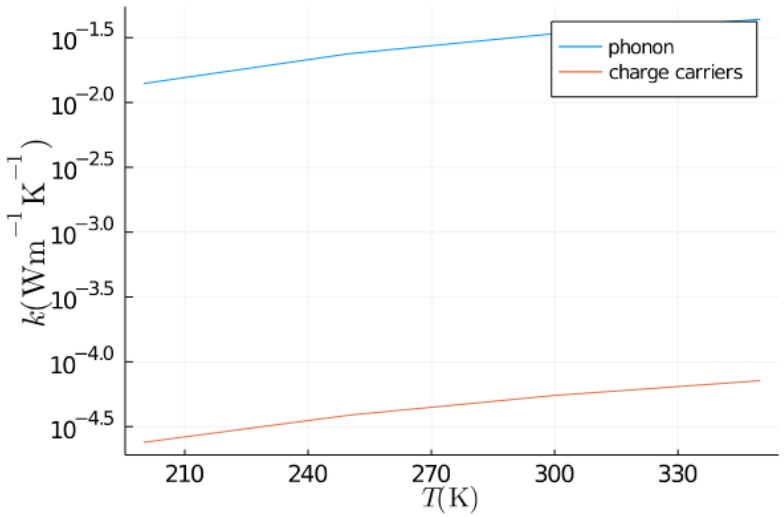

Figure 3.20: k dependence on T (pentacene $N_i = 3 \times 10^{21}\,\mathrm{cm}^{-3}$)

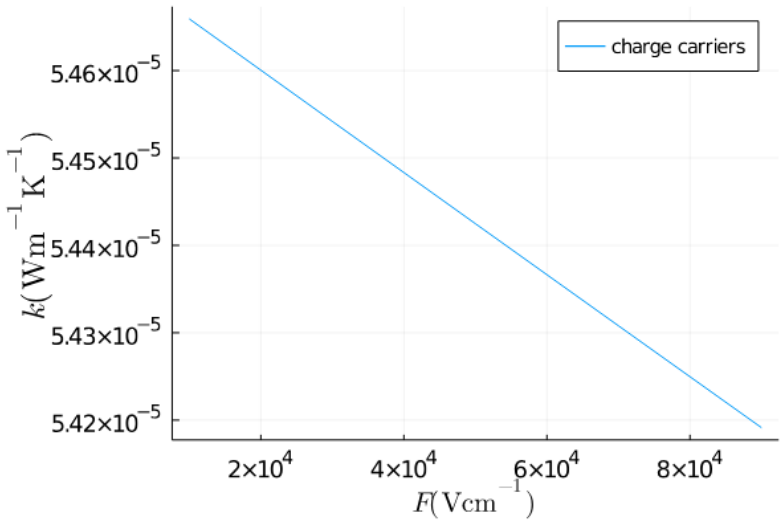

Figure 3.21: k dependence on F (pentacene $N_i = 3 \times 10^{21}\,\mathrm{cm}^{-3}$)

Semiconductor structure

There are multiple ways to change the structure of the semiconductor, i.e changing its DOS: density of states N_i, the doping N_d and the disorder σ.

From N_i standpoint, we see (fig. 3.22) that increasing state density means better

thermal conduction: a more dense network of states help the thermal conduction. This conclusion applies for both the phonons and charge carriers conduction. However, regarding the charge carrier one, the impact of the charge carrier on D could also mean that more charge carrier participates to the thermal conduction, and not only the addition of new states.

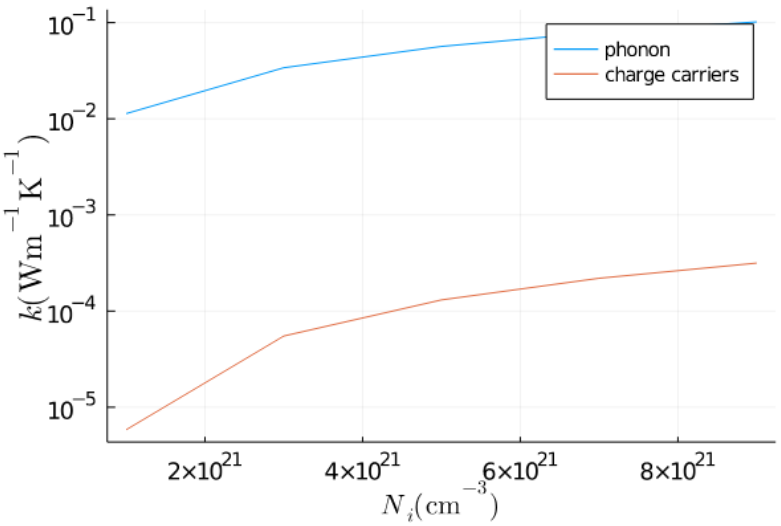

Figure 3.22: k dependence on N_i (pentacene, $F = 5.3 \times 10^4\,\mathrm{Vcm}^{-1}$)

Chapter 4

Julia implementation

4.1 Introduction

Julia is a recent open-source language (MIT) which has been developed specifically for scientific purposes. Syntax is also very similar to what can be done with Python, meaning that it's easy to read and write efficient code. Of course the syntax is also optimized for mathematics purpose, and the expressions are straightforwardly converted into the computer language. Even though it is a compiled language like Matlab, his use of REPL makes it quite easy to beta test code and run simple programs. The huge community involved around the language makes it easier to find useful package that are already optimized for fast computation in Julia. The support of other languages within the Julia language allows an even greater access to simple and user friendly tools: it is very easy to use the Python graphic renderer to plot and easily visualize data.

4.2 Performances

One key argument in choosing Julia over Matlab was its performances. According to the officials data (fig. 4.1), for this specific benchmark, Julia language reaches the performances of static-compiled languages such as C and is even better performing than Matlab.

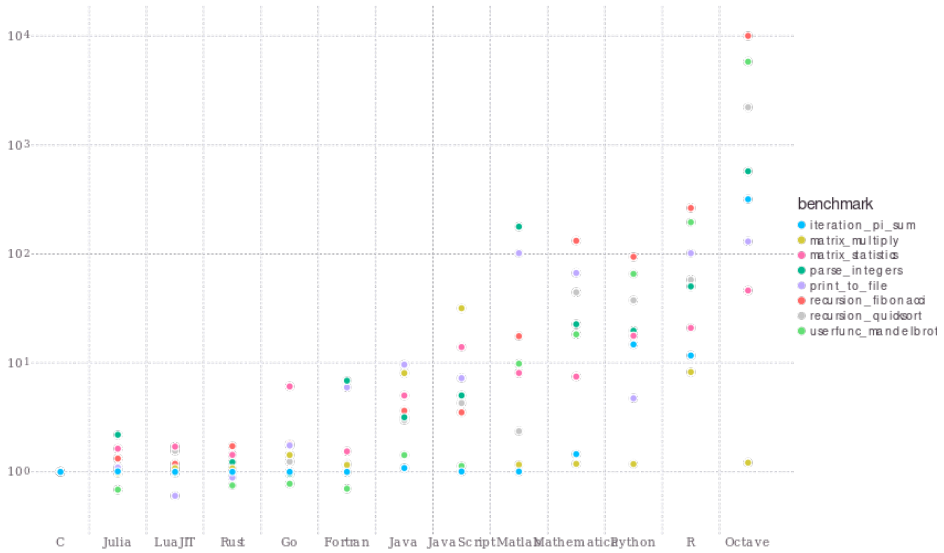

Figure 4.1: Julia benchmark

4.3 Notebooks

The communication and presentation of data and code is a key part in making a scientific work. To help smoothing out the process, we intensively used Jupyter notebooks. They put in the same document programming language code, as well as plain text (rendered through markdown) to help clarify and improve the overall lisibility.

4.4 Code implementation

4.4.1 Reduced quantities

To help facilitate the comprehension of each function, reduced quantities for the energy and the spatial coordinates have been used as functions parameters.

```
function xf(semiconductor::Semiconductor, U::Real, T::Real,
    F::Real)::Float64
    R = Conduction.RnnVRH(semiconductor, U, T, F);

    return xf(semiconductor, R, U, T, F)
```

```
    end
```

Typical functions for the diverse parameters are taking as parameters the semiconductor structure, energy, temperature and field intensity. Besides, we used extensively Julia's feature multiple dispatch to simplify and improve the readability of the function. For example in code 4.4.1, the primal function xf computes an other function xf with different parameters. By doing so we can maintain a coherent environment for the function calls, the real computation being done by:

```
function xf(semiconductor::Semiconductor, Rnn::Real, U::Real,
    T::Real, F::Real)
    functionI = [I1, I2, I3, I4]
    resultI = Array{Float64}(undef, 4)

    for i in 1:4
        resultI[i] = functionI[i](U, T, semiconductor, Rnn, F)
    end

    return (resultI[1] + resultI[2]) / (resultI[3] + resultI[4])
end
```

4.4.2 Range of computation

For many quantities (mobility 2.18, ...) a global value requires an integral over all the possible energies of the form:

$$h = \frac{\int_{-\infty}^{+\infty} g(u)F(U)h(u)}{\int_{-\infty}^{+\infty} g(u)F(U)} \tag{4.1}$$

However, in the eq. 4.1, the range of integration doesn't allow a smooth computation in a reasonable amount of time: usually $h(u)$ function is complicated equation involving most of the time other integrals. To reduce the time of computation, one has to first reduce the range of integration. Thankfully to our model and the gaussian DOS, most of the charge carrier are trapped in a certain energy range (fig. 4.2). Such range has to be investigated for each change of material. For example with the pentacene (parameters fig 4.2), we see that for an energy of

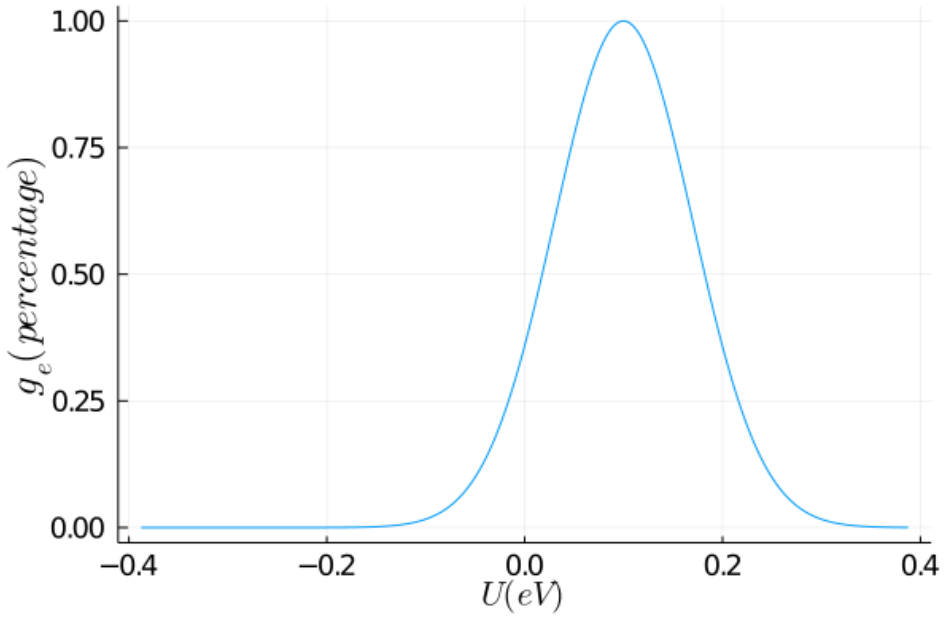

Figure 4.2: DOS compared to the maximum value

0.4 eV, we have roughly 0.002 % of carrier (100 % being the maximum value for $U = \hbar\omega_\alpha$).

4.4.3 Integration in Julia

One of the key aspect of the modelisation that has been performed, was to perform easily and quickly complex integral over multiple dimension. The computation of 1D expression such as k_p (eq. 3.5) has been realized using QUADGK package:

```
kp(semiconductor, T) = k * T * quadgk(
    r -> DOSp(semiconductor, r, T) * C(r, T) * Dp(semiconductor, r,
       T),
    semiconductor.omega_min * hbar / (k * T),
    +Inf
)[1]
```

The multidimensional integrals have been computed using HCubature:

```
# Number of free state within a sphere of radius R
```

```
N(semiconductor::Semiconductor, U::Real, T::Real, R::Real)::Float64
    = (k * T) / (8 * semiconductor.alpha^3) * 2 * pi * hcubature(
    x -> DOS(semiconductor, var1(U, semiconductor.beta(T), R, x[1],
        x[2], x[3]), T) * (1 - F(semiconductor, var1(U,
        semiconductor.beta(T), R, x[1], x[2], x[3]), T)) * 1 / (1 -
        x[1])^2 * x[2]^2 * sin(x[3]),
    [0, 0, 0],
    [1, R, pi],
    rtol=1e-6)[1]
```

However, concerning the multi-dimensional integrals, they can't be used as they were presented in the thesis. The parameters presented in the born have to be some constant and not depend on an other integral parameters.

Number of free states

The formula for the number of free state is taken from eq. 2.12 :

$$\mathcal{N}(u,T,\beta,\mathscr{R}) = \int_0^{\pi}\int_0^{\mathscr{R}}\int_{-\infty}^{\mathscr{R}+u-r(1+\beta\cos\theta)} g(v)\left[1-F(v)\right]\frac{kT}{8\alpha^3} \times 2\pi r^2\sin\theta\, dv\, dr\, d\theta \tag{4.2}$$

For the dv integrals, the superior born is defined by $\mathscr{R}+u-r(1+\beta\cos\theta)$, where θ and R' are already parameters for the first and second integral. In order to get rid of such born, we've made the change of variable:

$$v = \mathscr{R}+u-r(1+\beta\cos\theta) - \frac{t}{1-t} = a - \frac{t}{1-t} \tag{4.3}$$

It results in the change from eq. 4.2 to:

$$\mathcal{N}(u,T,\beta,\mathscr{R}) = \int_0^{\pi}\int_0^{\mathscr{R}}\int_0^{1} N\left(a-\frac{t}{1-t}\right)\left[1-F\left(a-\frac{t}{1-t}\right)\right]\frac{kT}{8\alpha^3} \times 2\pi r^2\sin\theta\frac{1}{(1-t)^2}\, dt\, dr\, d\theta \tag{4.4}$$

With this simple change of variable, the time of computation has been reduced from several minutes depending on the initial conditions, to a few seconds.

Real hopped distance

From the equation of the real hopped distance (eq. 2.14):

$$\begin{aligned}
I_1 &= \int_0^{\pi} \int_{u-\overline{r_{nn}}\beta\cos\theta}^{u+\overline{r_{nn}}} N(v)\left[1-F(v)\right]\left[\frac{\overline{r_{nn}}-v+u}{1+\beta\cos\theta}\right]^3 \times \sin\theta\cos\theta dv d\theta \\
I_2 &= \int_0^{\pi} \int_{-\infty}^{u-\overline{r_{nn}}\beta\cos\theta} N(v)\left[1-F(v)\right]\overline{r_{nn}}^3 \sin\theta\cos\theta dv d\theta \\
I_3 &= \int_0^{\pi} \int_{u-\overline{r_{nn}}\beta\cos\theta}^{u+\overline{r_{nn}}} N(v)\left[1-F(v)\right]\left[\frac{\overline{r_{nn}}-v+u}{1+\beta\cos\theta}\right]^2 \sin\theta dv d\theta \\
I_4 &= \int_0^{\pi} \int_{-\infty}^{u-\overline{r_{nn}}\beta\cos\theta} N(v)\left[1-F(v)\right]\overline{r_{nn}}^2 \sin\theta dv d\theta
\end{aligned} \tag{4.5}$$

Similarly to the section 4.4.3, the area of integrals contain integrated variable θ. By the change of variable for I_1 and I_3:

$$v = f_1(t) = \overline{\mathscr{R}_{nn}}\left[\frac{1+\beta\cos\theta}{t} - \beta\cos\theta\right] + u \tag{4.6}$$

And by doing the change of variable for I_2 and I_4:

$$v = f_2(t) = u - \overline{\mathscr{R}_{nn}}\beta\cos\theta - \frac{t}{1-t} \tag{4.7}$$

We obtain the following formulas:

$$
\begin{aligned}
I_1 &= 0.5 * \overline{r_{nn}} \int_0^{\pi} \int_0^1 N\left(f_1\left(t\right)\right)\left[1 - F\left(f_1\left(t\right)\right)\right] \frac{\left[\overline{r}_{nn} - f_1\left(t\right) + u\right]^3}{\left[1 + \beta\cos\theta\right]^2} \sin(2\theta) dt d\theta \\
I_2 &= 0.5 * \overline{r_{nn}}^3 \int_0^{\pi} \int_0^1 N\left(f_2\left(t\right)\right)\left[1 - F\left(f_2\left(t\right)\right)\right] \sin(2\theta) \frac{1}{\left(1-t\right)^2} dt d\theta \\
I_3 &= \overline{r_{nn}} \int_0^{\pi} \int_0^1 N\left(f_1\left(t\right)\right)\left[1 - F\left(f_1\left(t\right)\right)\right] \frac{\left[\bar{r}_{nn} - f_1\left(t\right) + u\right]^2}{\left[1 + \beta\cos\theta\right]} \sin(\theta) dt d\theta \\
I_4 &= \overline{r_{nn}}^2 \int_0^{\pi} \int_0^1 N\left(f_2\left(t\right)\right)\left[1 - F\left(f_2\left(t\right)\right)\right] \sin(\theta) \frac{1}{\left(1-t\right)^2} dt d\theta
\end{aligned}
\tag{4.8}
$$

Stochastic time of release

From the equation of the stochastic time of release (eq. 2.22):

$$
\begin{aligned}
J_1\left(u\right) &= \int_0^{\pi} d\theta \sin\theta \int_0^{\overline{r_{nn}}} dr 2\pi r^2 \int_{u - r\beta\cos\theta}^{\overline{r_{nn}} + u - r(1+\beta\cos\theta)} du \\
&\quad \times \frac{\tau\left(u, u_F\right)}{v_0} \exp\left(\left(1 + \beta\cos\theta\right)r + u - u\right), \\
J_2\left(u\right) &= \int_0^{\pi} d\theta \sin\theta \int_0^{\overline{r_{nn}}} dr 2\pi r^2 \int_{-\infty}^{u - r\beta\cos\theta} du \frac{\tau\left(u, u_F\right)}{v_0} \\
&\quad \times \exp((1 + \beta\cos\theta)r), \\
J_3\left(u\right) &= \int_0^{\pi} d\theta \sin\theta \int_0^{\overline{r_{nn}}} dr 2\pi r^2 \int_{u - r\beta\cos\theta}^{\overline{r_{nn}} + u - r(1+\beta\cos\theta)} du \tau\left(u, u_F\right), \\
J_4\left(u\right) &= \int_0^{\pi} d\theta \sin\theta \int_0^{\overline{r_{nn}}} dr 2\pi r^2 \int_{-\infty}^{u - r\beta\cos\theta} du \tau\left(u, \epsilon_F\right)
\end{aligned}
\tag{4.9}
$$

By doing the change of variable for J_1 and J_3:

$$
v = g_1\left(t\right) = t\left(\overline{r_{nn}} - r\right) + u + r\beta\cos\theta \tag{4.10}
$$

And by doing the change of variable for J_2 and J_4:

$$
g_2\left(t\right) = \frac{t}{t-1} + u - r\beta\cos\theta \tag{4.11}
$$

We obtain the following formulas:

$$
\begin{aligned}
I_1(u) &= \int_0^{\pi} d\theta \sin\theta \int_0^{\overline{r_{nn}}} dr 2\pi r^2 \int_0^1 dt \frac{\tau\left(g_1(t), u_F\right)}{v_0} \exp\left((1+\beta\cos\theta)r + g_1(t) - u\right) \\
I_2(u) &= \int_0^{\pi} d\theta \sin\theta \int_0^{\overline{r_{nn}}} dr 2\pi r^2 \int_0^1 dt \frac{\tau\left(g_2(t), u_F\right)}{v_0} \exp((1+\beta\cos\theta)) \\
I_3(u) &= \int_0^{\pi} d\theta \sin\theta \int_0^{\overline{r_{nn}}} dr 2\pi r^2 \int_0^1 dt \tau\left(g_1(t), u_F\right) \\
I_4(u) &= \int_0^{\pi} d\theta \sin\theta \int_0^{\overline{r_{nn}}} dr 2\pi r^2 \int_0^1 dt \tau\left(g_2(t), u_F\right)
\end{aligned}
\tag{4.12}
$$

4.5 Conclusion

Thanks to the possibilities of Julia and to numerous package, we could optimize the code to obtain a final computation of einstein ratio in the order of several minutes/hours depending on the initial conditions.

Optimization is a key point to computational simulation as we need to get a result in a fair amount of time in order to work by iteration and tune our model to real data: we may want to fit a certain numerical value for instance.

Chapter 5

Conclusion

5.1 Discussion

The electric model that we developed offered results in range with the previous literature, while giving some change in behavior and tendency. We could conclude that the geometry of the DOS and the density of charge carriers were playing a great role in understanding the behavior of the diffusion D and the mobility μ. It seems that the diffusivity is very sensitive to DOS geometry and μ to charge carrier quantity. With an increase in the number of free state, the global Einstein ratio η was experiencing an increase, meaning that the diffusion was becoming preponderant in the material compared to the diffusivity. This effect was quite striking with the increase of energetic disorder.

Such conclusion can be applied to doping. The process of doping alters greatly the structure of the DOS by bringing new states and by reducing the influence of traps and increases more efficiently the diffusion process and the Einstein ratio. However, the effect of increasing the doping does not change the DOS structure in such way and the increase in charge carrier becomes more preponderant regarding the Einstein ratio behavior, reducing it.

Our model described behavior that is consistent and matches the behavior of other models found in literature. The final range of electric mobility, conduction and Einstein ratio are coherent with precedent work and give reasonable approximation. But some aspects still need to be better explained: the Einstein ratio experiencing a local maximum at low temperature, as well as the local maximum regarding the field.

Regarding the thermal conduction, our model described values in range with precedent work for the phonon transports, but yielded overwhelmingly low values for the charge carrier thermal conduction, as well as a strange dependency regarding the field. It has been concluded that the computation precision is not adequate for such computation as the variations of the integrated quantity are very high.

The implementation of this new model on Julia as also been successful. Our model can produce results in few minutes for a reasonable range of parameters on different computers. We took great care in producing a readable and understandable code to facilitate the comprehension and usability of the implemented model.

5.2 Limits

As explained in the chapter 2, we made many assumptions and approximation on the diffusion quantity. Trapping effect has also been taken into account solely for the diffusion.

Most important, the data retrieved from precedent studies may be difficult to incorporate in our model, as the quality of the probing and the correspondences with our model may be hard to find.

5.3 Future prospects

An in-depth inspection of the assumption made for the diffusivity may be needed to better understand the process behind the diffusion. Even though our result were in range with precedent work, a more refined model may be considered.

As reported earlier, the trapping effect is not really considered for the mobility and the addition of an exponential DOS in top of the Gaussian DOS could be a solution into reducing the too-high mobility obtained for pentacene.

Thermal conduction needs to be better understood in order to produce a more accurate description of phonon diffusion. Besides, the charge carrier phonon transport is not satisfactory and need some changes to produce values in range with the literature, as well as more coherent behavior regarding the field intensity.

The overall model in Julia still have some accuracy problems, particularly for

extreme values and for very high or low energies (at several electron volts). A better understanding of the model at extreme energies could help refine the model and improve the overall precision.

References

[1] Apsley, N., and Hughes, H. P. Temperature-and field-dependence of hopping conduction in disordered systems. *The Philosophical Magazine: A Journal of Theoretical Experimental and Applied Physics 30*, 5 (1974), 963–972.

[2] Apsley, N., and Hughes, H. P. Temperature- and field-dependence of hopping conduction in disordered systems, ii. *The Philosophical Magazine: A Journal of Theoretical Experimental and Applied Physics 31*, 6 (1975), 1327–1339.

[3] Bakulin, A., Lovrincic, R., Yu, X., Selig, O., Bakker, H., Rezus, Y., Nayak, P., Fonari, A., Coropceanu, V., Brédas, J.-L., and Cahen, D. Mode-selective vibrational modulation of charge transport in organic electronic devices. *Nature Communications 6* (08 2015), 7880.

[4] Baranovskii, S., Faber, T., Hensel, F., Thomas, P., and Adriaenssens, G. Einstein's relationship for hopping electrons. *Journal of Non-Crystalline Solids 198-200* (1996), 214–217. Proceedings of the Sixteenth International Conference on Amorphous Semiconductors - Science and Technology.

[5] Berman, R. *Thermal Conduction in Solids*. OXFORD SCIENCE PUBLICATIONS. Clarendon Press, 1979.

[6] Brütting, W. Introduction to the physics of organic semiconductors. 1–14.

[7] Bässler, H. Charge transport in disordered organic photoconductors a monte carlo simulation study. *physica status solidi (b) 175*, 1 (1993), 15–56.

[8] Chiang, C. K., Fincher, C. R., Park, Y. W., Heeger, A. J., Shirakawa, H., Louis, E. J., Gau, S. C., and MacDiarmid, A. G. Electrical conductivity in doped polyacetylene. *Phys. Rev. Lett. 39* (Oct 1977), 1098–1101.

[9] Einstein, A. Über die von der molekularkinetischen Theorie der Wärme geforderte Bewegung von in ruhenden Flüssigkeiten suspendierten Teilchen. *Annalen der Physik 322*, 8 (Jan. 1905), 549–560.

[10] Einstein, A. Elementare betrachtungen über die thermische molekularbewegung in festen körpern [adp 35, 679 (1911)]. *Annalen der Physik 14*, S1 (2005), 408–424.

[11] Feldman, J. L., Kluge, M. D., Allen, P. B., and Wooten, F. Thermal conductivity and localization in glasses: Numerical study of a model of amorphous silicon. *Phys. Rev. B 48* (Nov 1993), 12589–12602.

[12] Kempa, X. Study of the impact of einstein relation enhancement on organic diodes in the case of variable range hopping. Master's thesis, Keio University Graduate School of Science and Technology School of Integrated Design Engineering, 2020.

[13] Li, L., Lu, N., Liu, M., and Bässler, H. General einstein relation model in disordered organic semiconductors under quasiequilibrium. *Phys. Rev. B 90* (Dec 2014), 214107.

[14] Liu, C., Huang, K., Park, W.-T., Li, M., Yang, T., Liu, X., Liang, L., Minari, T., and Noh, Y.-Y. A unified understanding of charge transport in organic semiconductors: the importance of attenuated delocalization for the carriers. *Mater. Horiz. 4* (2017), 608–618.

[15] Lu, N., Li, L., Gao, N., and Liu, M. A unified description of thermal transport performance in disordered organic semiconductors. *Organic Electronics 41* (2017), 294–300.

[16] Lu, N., Li, L., Gao, N., and Liu, M. A unified description of thermal transport performance in disordered organic semiconductors. *Organic Electronics 41* (2017), 294–300.

[17] Miller, A., and Abrahams, E. Impurity conduction at low concentrations. *Phys. Rev. 120* (Nov 1960), 745–755.

[18] Minamiki, T., Minami, T., Chen, Y.-P., Mano, T., Takeda, Y., Fukuda, K., and Tokito, S. Flexible organic thin-film transistor immunosensor printed on

a one-micron-thick film. *Communications Materials 2* (01 2021).

[19] Mitzi, D. B. Synthesis, structure, and properties of organic-inorganic perovskites and related materials. 1–121.

[20] Nenashev, A. V., Jansson, F., Baranovskii, S. D., Österbacka, R., Dvurechenskii, A. V., and Gebhard, F. Effect of electric field on diffusion in disordered materials. ii. two- and three-dimensional hopping transport. *Phys. Rev. B 81* (Mar 2010), 115204.

[21] Richert, R., Pautmeier, L., and Bässler, H. Diffusion and drift of charge carriers in a random potential: Deviation from einstein's law. *Phys. Rev. Lett. 63* (Jul 1989), 547–550.

[22] Roichman, Y., and Tessler, N. Generalized einstein relation for disordered semiconductors—implications for device performance. *Applied Physics Letters 80*, 11 (2002), 1948–1950.

[23] Sandanayaka, A. S. D., Matsushima, T., Bencheikh, F., Terakawa, S., Potscavage, W. J., Qin, C., Fujihara, T., Goushi, K., Ribierre, J.-C., and Adachi, C. Indication of current-injection lasing from an organic semiconductor. *Applied Physics Express 12*, 6 (may 2019), 061010.

[24] Schirmacher, W., Diezemann, G., and Ganter, C. Harmonic vibrational excitations in disordered solids and the "boson peak". *Phys. Rev. Lett. 81* (Jul 1998), 136–139.

[25] Shaw, J., and Seidler, P. Organic electronics: Introduction. *IBM Journal of Research and Development 45* (02 2001), 3 – 9.

[26] Shenogin, S., Bodapati, A., Keblinski, P., and McGaughey, A. J. H. Predicting the thermal conductivity of inorganic and polymeric glasses: The role of anharmonicity. *Journal of Applied Physics 105*, 3 (2009), 034906.

[27] Shenogin, S., Bodapati, A., Keblinski, P., and McGaughey, A. J. H. Predicting the thermal conductivity of inorganic and polymeric glasses: The role of anharmonicity. *Journal of Applied Physics 105*, 3 (2009), 034906.

[28] Shibata, M., Sakai, Y., and Yokoyama, D. Advantages and disadvantages of

vacuum-deposited and spin-coated amorphous organic semiconductor films for organic light-emitting diodes. *J. Mater. Chem. C 3* (2015), 11178–11191.

[29] Stehr, V. *Prediction of charge and energy transport in organic crystals with quantum chemical protocols employing the hopping model*. PhD thesis, 06 2015.

[30] Tal, O., Epstein, I., Snir, O., Roichman, Y., Ganot, Y., Chan, C. K., Kahn, A., Tessler, N., and Rosenwaks, Y. Measurements of the einstein relation in doped and undoped molecular thin films. *Phys. Rev. B 77* (May 2008), 201201.

[31] Wyart, M. Scaling of phononic transport with connectivity in amorphous solids. *EPL (Europhysics Letters) 89*, 6 (Mar 2010), 64001.

[32] Zhang, X., Dong, H., and Hu, W. Organic semiconductor single crystals for electronics and photonics. *Advanced Materials 30*, 44 (2018), 1801048.

[33] Zschieschang, U., Borchert, J. W., Giorgio, M., Caironi, M., Letzkus, F., Burghartz, J. N., Waizmann, U., Weis, J., Ludwigs, S., and Klauk, H. Roadmap to gigahertz organic transistors. *Advanced Functional Materials 30*, 20 (2020), 1903812.

Appendix

A Pentacene characteristics

The following values have been taken from the precedent work of Xavier [12] for pristine pentacene:

- $\alpha = 4.34 \times 10^7\,\mathrm{cm}^{-1}$
- $\sigma = 0.071\,\mathrm{eV}$
- $E_F = -0.7\,\mathrm{eV}$
- $\nu_0 = 1 \times 10^{13}\,\mathrm{Hz}$

B Doped α-NPD

- $\alpha = 4.34 \times 10^7\,\mathrm{cm}^{-1}$
- $\sigma_i = 0.1\,\mathrm{eV}$
- $\sigma_i = 0.1\,\mathrm{eV}$
- $E_F = -0.62\,\mathrm{eV}$
- $\nu_0 = 1 \times 10^{13}\,\mathrm{Hz}$